Nucleic Acids Research, 2023 **1**
https://doi.org/10.1093/nar/gkac1261

Molecular architecture and oligomerization of *Candida glabrata* Cdc13 underpin its telomeric DNA-binding and unfolding activity

Javier Coloma[1,*,†], Nayim Gonzalez-Rodriguez[1,†], Francisco A. Balaguer[2], Karolina Gmurczyk[2], Clara Aicart-Ramos[2], Óscar M. Nuero[3], Juan Román Luque-Ortega[3], Kimberly Calugaru[4], Neal F. Lue[4], Fernando Moreno-Herrero[2,*] and Oscar Llorca[1,*]

[1]Structural Biology Programme, Spanish National Cancer Research Centre (CNIO), Madrid, Spain, [2]Department of Macromolecular Structures, Centro Nacional de Biotecnología, Consejo Superior de Investigaciones Científicas, Madrid, Spain, [3]Molecular Interactions Facility, Centro de Investigaciones Biológicas Margarita Salas (CSIC), Madrid, Spain and [4]Department of Microbiology and Immunology, W. R. Hearst Microbiology Research Center, Weill Cornell Medicine, New York, NY, USA

Received May 27, 2022; Revised December 14, 2022; Editorial Decision December 15, 2022; Accepted December 19, 2022

ABSTRACT

The CST complex is a key player in telomere replication and stability, which in yeast comprises Cdc13, Stn1 and Ten1. While Stn1 and Ten1 are very well conserved across species, Cdc13 does not resemble its mammalian counterpart CTC1 either in sequence or domain organization, and Cdc13 but not CTC1 displays functions independently of the rest of CST. Whereas the structures of human CTC1 and CST have been determined, the molecular organization of Cdc13 remains poorly understood. Here, we dissect the molecular architecture of *Candida glabrata* Cdc13 and show how it regulates binding to telomeric sequences. Cdc13 forms dimers through the interaction between OB-fold 2 (OB2) domains. Dimerization stimulates binding of OB3 to telomeric sequences, resulting in the unfolding of ssDNA secondary structure. Once bound to DNA, Cdc13 prevents the refolding of ssDNA by mechanisms involving all domains. OB1 also oligomerizes, inducing higher-order complexes of Cdc13 *in vitro*. OB1 truncation disrupts these complexes, affects ssDNA unfolding and reduces telomere length in *C. glabrata*. Together, our results reveal the molecular organization of *C. glabrata* Cdc13 and how this regulates the binding and the structure of DNA, and suggest that yeast species evolved distinct architectures of Cdc13 that share some common principles.

INTRODUCTION

Telomeres are structures formed at the end of the linear chromosomes in eukaryotes, consisting of DNA repeats bound by multiple protein complexes. Telomeric DNA is comprised of numerous copies of a short, double stranded repeat, which terminates in a single-stranded 3′ overhang, known as the G-overhang. Telomeres prevent the ends of chromosomes from being recognized as double strand breaks by the cellular DNA repair machinery (1) and from the shortening of chromosome ends upon genome replication (2). Thus, telomere regulation and maintenance are crucial pathways to prevent genomic instability, which is linked to many complex diseases including cancer and ageing (3,4).

CST, the complex formed by Cdc13-Stn1-Ten1 in yeast and CTC1-STN1-TEN1 in humans, is required for telomere maintenance and protection. In yeast, telomere capping through the binding to the G-overhang and the regulation of telomere replication are the best characterized functions of CST (4–6). In the budding yeast *Saccharomyces cerevisiae*, CST directly interacts with the Est1 subunit of telomerase, the complex that elongates the G-strand, through its recruitment domain (RD) (7,8) and with the catalytic subunit of the DNA polymerase alpha (Pol α), which is in charge of C-strand fill-in (9,10). CST stimulates Pol α by promoting RNA priming and the transfer of the newly synthesized RNA from the primase subunits to the polymerase subunit (11). The direct binding to telomerase and Pol α places CST at the center of the mechanisms that regulate replication of both telomeric strands. In addition, CST participates in other functions, at least in mammalian

*To whom correspondence should be addressed. Tel: +34 91 732 8000 (Ext 3000); Email: ollorca@cnio.es
Correspondence may also be addressed to Javier Coloma. Tel: +34 91 732 8000 (Ext 3033); Email: jcoloma@cnio.es
Correspondence may also be addressed to Fernando Moreno-Herrero. Tel: +34 91 585 5305; Email: fernando.moreno@cnb.csic.es
†The authors wish it to be known that, in their opinion, the first two authors should be regarded as Joint First Authors.

cells, such as DNA repair (12–16), chromosome cohesion (17), and helping the cells manage DNA replication stress (18,19).

While Stn1 and Ten1 are very well conserved across species (20), Cdc13 has been proposed to be the ortholog of human CTC1 despite showing only partial resemblance in domain organization and little sequence conservation (21,22). Human CTC1 is a 1217 amino acid protein harboring seven oligonucleotide/oligosaccharide-binding fold (OB-fold) domains (21), whereas *S. cerevisiae* Cdc13 is much smaller, with 924 amino acids spanning four OB-fold domains and a disordered telomerase-recruiting RD domain placed between the first and second OB-fold domains (OB1 and OB2) (23,24) (Figure 1A). In addition, yeast Cdc13 can perform functions on its own and independently of Stn1 and Ten1 (25,26), while there is no evidence that supports an independent activity of CTC1. Indeed, Cdc13 dissociates from Stn1-Ten1 and interacts with the Est1 subunit of yeast telomerase in late S phase when the level of Est1 rises (27). Moreover, although Cdc13, Stn1 and Ten1 form a complex, yeast Cdc13 has a predominant role in inhibiting telomere fusion over Stn1 and Ten1 (25).

Significant progress has been recently made on the structural characterization of human CST and its complex with Pol α using cryo-electron microscopy (cryoEM) (21,28,29). The cryoEM structures revealed the organization of seven OB-fold domains of CTC1, with OB-fold domains D, E, F and G forming a ring that interacts with STN1-TEN1 in a 1:1:1 stoichiometry. In addition, human CST assembles a large decameric complex upon interaction with telomeric ssDNA (21). When Flag-tagged and V5-tagged CTC1 are co-expressed, either tag immunoprecipitates the other and this has been interpreted as proof that higher-order CST oligomeric species form in human cells and could have functional significance (21). Formation of oligomeric Cdc13 complexes have also been suggested to explain how *S. cerevisiae* Cdc13 shortened DNA in experiments using single-molecule methods (30).

In contrast to human CST, the available information about the structure of Cdc13 and yeast CST is rather incomplete and, in some cases, contradictory. Budding yeast Cdc13 has been proposed to act as a homodimer, but the exact mode of dimerization is still a subject of debate. *S. cerevisiae* OB1 and OB2 domains form dimers when isolated, and the structures of these dimers have been determined by X-ray crystallography (10,23,24). The dimerization via OB2 was found to be important for binding to Stn1 and for telomere maintenance (23) but mutations in *S. cerevisiae* OB1 are sufficient to disrupt Cdc13 dimers without influencing ssDNA binding (31). *Candida glabrata* OB4 domain also forms dimers when studied separately from the rest of Cdc13, and their crystal structure revealed that OB4 uses a different mechanism for dimerization than OB2 (22). Several models have been proposed for how Cdc13 assembles the CST complex. Crystal structures of fragments of the *Kluyveromyces lactis* homologs suggested that dimerization of Cdc13 is mediated by Stn1 in the context of CST, and Stn1 bridges OB2 and OB4 domains from two Cdc13 subunits (32). In contrast, work on *C. glabrata* pointed to various unusual stoichiometries for Cdc13, Stn1 and Ten1 (2:4:2 or 2:6:2) (33).

Overall, the structural organization and mode of oligomerization of yeast Cdc13 as well as how these features could influence its DNA binding activity, is still poorly characterized. Furthermore, discrepancies between several reports are difficult to reconcile into a single structural and architectural model. In this study, we have clarified the molecular organization and the mechanisms of oligomerization of *C. glabrata* Cdc13 by applying multiple biochemical and biophysical techniques on a collection of constructs. This species was selected as it contains the only yeast CST complex where all three full-length subunits of CST can be expressed and reconstituted through a recombinant system (33). We have determined that *C. glabrata* Cdc13 forms a dimeric complex that only requires the dimerization of OB2, and this dimerization enhances binding to telomeric sequences. Single-molecule experiments using magnetic tweezers demonstrated that Cdc13 unfolds ssDNA secondary structures and, once bound to DNA, Cdc13 prevents its refolding. Although OB3 binds telomeric sequences on its own, OB3 alone is unable to prevent the refolding of ssDNA, and each domain in Cdc13 contributes to modifying the structure of ssDNA. In addition, we find that OB1 induces the formation of large oligomers of Cdc13 formed by the stepwise addition of Cdc13 dimers, and we have mapped residues required for OB1 oligomerization using mutational analysis. Our data is consistent with previous findings on the oligomerization of yeast Cdc13 (24,30,34) and human CST (21). Thus, we speculate that the ability of OB1 to direct the interaction of several Cdc13 dimers may play a role in altering the structure of ssDNA. Altogether, we propose the first detailed model for the molecular architecture of *C. glabrata* Cdc13 and how its structural organization impacts on the binding to ssDNA.

MATERIALS AND METHODS

ORF cloning

All cloning, subcloning and site-directed mutagenesis steps were performed using IVA cloning (35). The ORF of *C. glabrata* full-length Cdc13 (UniProtKB - Q6FT40) was amplified by PCR from the previously described pACYCDuet-Cdc13FLAG plasmid (33) and inserted into pDV1BUK-C2 plasmid (Trialtus Bioscience), to which we fused two Strep-Tag sequences and a TEV cleavage site by site-directed mutagenesis in the N-terminus. The resultant pDV1BUK-C2-Strep-Cdc13 plasmid encoded for a Strep-Trx-CL7-SUMO-TEV-Strep-Cdc13 fusion protein.

Using site-directed mutagenesis and the pDV1BUK-C2-Strep-Cdc13 as a template we first removed the Trx-CL7-SUMO coding region and then the corresponding OB-fold domains to generate the pDV1-Strep-Cdc13, pDV1-Strep-Cdc13$_{OB1}$, pDV1-Strep-Cdc13$_{OB2}$, pDV1-Strep-Cdc13$_{OB3}$ and pDV1-Strep-Cdc13$_{OB4}$ which encode for the Strep-TEV-Strep-Cdc13 (residues 1–753), Strep-TEV-Strep-OB1 (residues 1–176), Strep-TEV-Strep-OB2 (260–396), Strep-TEV-Strep-OB3 (401–593) and Strep-TEV-Strep-OB4 (605–753) polypeptides, respectively. The deletion of the C-terminal region of OB1 (156–176) to generate pDV1-Strep-Cdc13$_{OB1\Delta C\text{-}ter}$ was performed using pDV1-Strep-Cdc13$_{OB1}$ as template. All point mutations

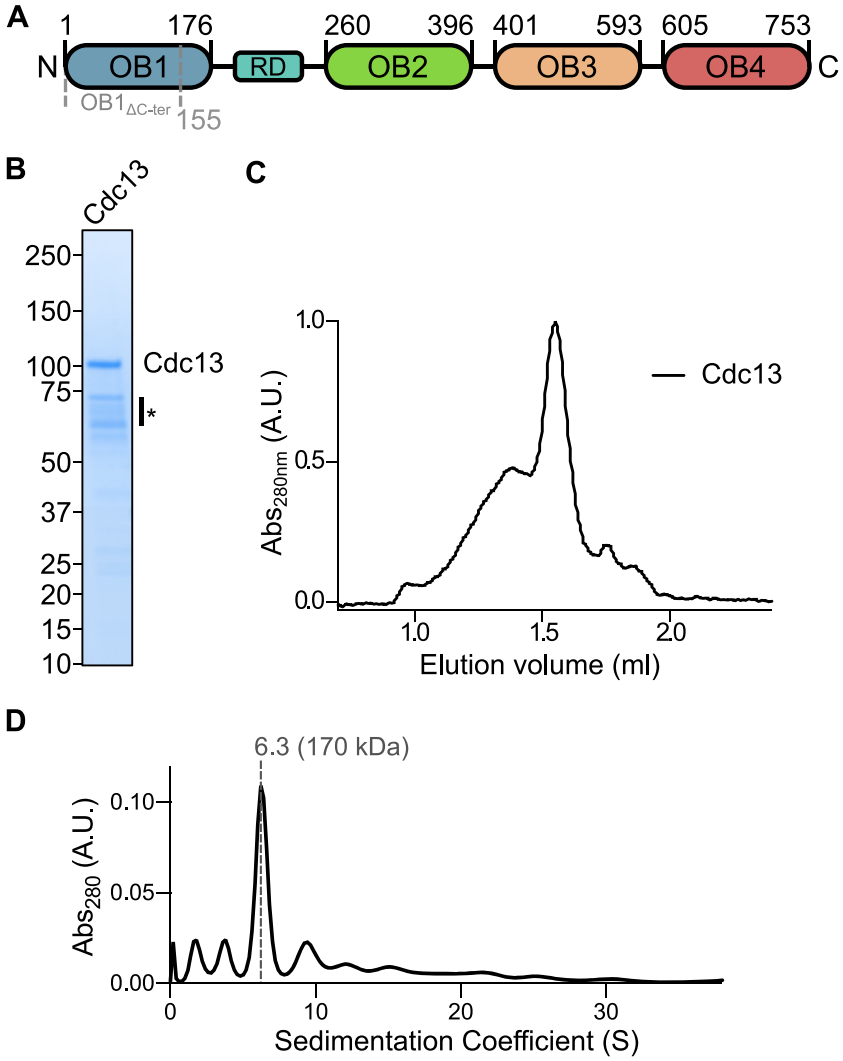

Figure 1. Purified recombinant *C. glabrata* Cdc13 forms dimers as well as larger oligomeric species in solution. (**A**) Schematic diagram of the arrangement of Cdc13 domains. (**B**) SDS-PAGE analysis of purified Cdc13. * Indicates minor bands corresponding to degradation products. (**C**) Superose 6 Increase SEC elution profile of Cdc13. The wide peak in early elution volumes corresponds to multimeric forms of Cdc13. (**D**) AUC analysis of the major peak of Cdc13 after SEC showing a mainly dimeric specie.

were again performed by site-directed mutagenesis using pDV1-Strep-Cdc13$_{OB1\Delta C\text{-ter}}$ as template.

Similarly, the pDV1BUK-C2-Strep-Cdc13 plasmid was modified by site-directed mutagenesis to individually remove OB folds 1 to 4 and generate the plasmids pDV1BUK-C2-Strep-Cdc13$_{OB234}$, pDV1BUK-C2-Strep-Cdc13$_{OB134}$, pDV1BUK-C2-Strep-Cdc13$_{OB124}$ and pDV1BUK-C2-Strep-Cdc13$_{OB123}$. These plasmids encode the Strep-Trx-CL7-SUMO-TEV-Strep-Cdc13$_{OB234}$, Strep-Trx-CL7-SUMO-TEV-Strep-Cdc13$_{OB134}$, Strep-Trx-CL7-SUMO-TEV-Strep-Cdc13$_{OB124}$ and Strep-Trx-CL7-SUMO-TEV-Strep-Cdc13$_{OB123}$ fusion proteins.

We subcloned the Cdc13$_{OB234}$ ORF into a modified pCDFDuet, and OB folds 2, 3 and 4 were individually removed by site-directed mutagenesis to produce the pCDF-H10-TEV-Cdc13$_{OB23}$, pCDF-H10-TEV-Cdc13$_{OB24}$ and pCDF-H10-TEV-Cdc13$_{OB34}$ vectors which encode for the H10-TEV-Cdc13$_{OB23}$, H10-TEV-Cdc13$_{OB24}$ and H10-TEV-Cdc13$_{OB34}$ polypeptides.

The ORFs of *C. glabrata* full-length Snt1 (A0A0W0D7U7) and Ten1 (UPI000C031EEB) were amplified from previously described pSMT3-Stn1 and pGEX6P-Ten1 plasmids respectively (33). The two ORFs were cloned into a pCDFDuet vector. A 10xHis tag, followed by a TEV cleavage site was fused to the N-terminus of Snt1 by site-directed mutagenesis.

Protein expression and purification

All constructs were expressed in BL21 (DE3) *Escherichia coli* cells (NZYTech) grown in ZYM-5052 auto-induction medium (36). After 5 h of growth at 37°C and 250 rpm, temperature was switched to 20°C and cells were left growing overnight. Cells spun down at 12 000 *g* during 10 min at 4°C, and the pellets were immediately lysed for purification or stored at −80°C.

The pellets were resuspended in lysis buffer (50 mM Tris–HCl pH 8.0, 50–200 mM NaCl, 10% (v/v) glycerol) sup-

plemented with a cocktail of proteases inhibitors (cOmplete EDTA-free, Roche), benzonase (2.5 U/ml) (Merck) and lysozyme (0.1 mg/ml) (Sigma-Aldrich). Cells were lysed by sonication and clarified by centrifugation at 50 000 g for 1 h at 4°C. Supernatants containing soluble proteins were filtered using through a 0.45 μm filter. The lysate containing 10xHis-TEV-Stn1-Ten1 was loaded onto a HisTrap HP affinity column (GE Healthcare) equilibrated in buffer A (50 mM Tris–HCl pH 8.0, 50 mM NaCl, 50 mM imidazole). Elution was performed using a gradient of increasing concentrations of imidazole with buffer B (50 mM Tris–HCl pH 8.0, 50 mM NaCl, 500 mM imidazole). Fractions containing purified 10xHis-TEV-Stn1-Ten1 were pooled and dialyzed in buffer A while cleaving with TEV protease at 4°C overnight. The cleaved sample was applied again onto a HisTrap HP column (GE Healthcare) equilibrated in buffer A. The flowthrough from the column was collected and loaded onto a HiTrap HP Q column (GE Healthcare) to remove nucleic acids. Bound proteins were eluted in a gradient with increasing concentrations of NaCl using buffer QB (50 mM Tris–HCl pH 8.0, 1 M NaCl).

To purify the Strep-TEV-Strep tag-containing constructs (Cdc13, OB1, OB2, OB3 and OB4) the corresponding lysates were loaded onto a Strep-Tactin XT Superflow High-Capacity Cartridge (IBA biosciences) equilibrated in Strep buffer A (50 mM Tris–HCl pH 8.0, 50 mM NaCl). Step elution was performed using Strep buffer A supplemented with 50 mM biotin. Fractions containing purified samples were pooled and applied to a HiTrap HP Q column (GE Healthcare) equilibrated in buffer A and eluted in a gradient with increasing concentrations of NaCl using buffer QB. For the mutational analysis of OB1, both the wild-type OB1 and all mutants were concentrated right after eluting from the affinity chromatography step described above.

To purify the constructs containing the Strep-Trx-CL7-SUMO-TEV-Strep tag (CST, $Cdc13_{OB234}$, $Cdc13_{OB134}$, $Cdc13_{OB124}$ and $Cdc13_{OB123}$) we used the same strategy as described above to purify the Strep-TEV-Strep constructs with an additional step to remove the tag. Eluates from the Strep-Tactin column were incubated overnight with TEV protease and applied to a Im7 4B FPLC Column (Trialtus Bioscience). The flowthrough from the column, containing cleaved samples, was collected and applied on a HiTrap HP Q column (GE Healthcare) to ensure removal of nucleic acids. In all cases, fractions containing purified samples were pooled together and immediately used for experiments or snap frozen in liquid N_2 and stored at −80°C.

Size-exclusion chromatography (SEC)

SEC analyses of the CST, Cdc13 and ST were performed in a Superose 6 3.2/300 Increase (Cytiva) previously equilibrated in 50mM Tris pH 8, 50 mM NaCl. The $Cdc13_{OB234}$, $Cdc13_{OB134}$, $Cdc13_{OB124}$ and $Cdc13_{OB123}$ constructs were also analyzed in the same column to compare the formation of higher-order multimers with Cdc13. For the individual OB folds, the analyses were performed in either a Superdex 75 10/300 Increase GL or a Superdex 200 3.2/300 Increase equilibrated in SEC buffer (25 mM Tris pH 7.5, 150 mM NaCl, 0.5 mM DTT). The $Cdc13_{OB23}$, $Cdc13_{OB24}$ and $Cdc13_{OB34}$ were run on a Superdex 200 3.2/300 Increase column equilibrated in PBS.

Coexpression and sequential pulldown experiments

The pDV1BUK-C2-Strep-$Cdc13_{OB234}$ plasmid was co-transformed in BL21(DE3) cells together with either the pCDF-H10-TEV-$Cdc13_{OB234}$, pCDF-H10-TEV-$Cdc13_{OB23}$, pCDF-H10-TEV-$Cdc13_{OB24}$ or pCDF-H10-TEV-$Cdc13_{OB34}$, grown and lysed as explained above. Cleared lysates were incubated with 100 μl of Ni^{2+}-NTA (Qiagen) resin for 30 min. The resin was washed with 5 × 1 ml wash buffer (50 mM Tris pH 8, 300 mM NaCl, 5% glycerol, 50 mM imidazole) and bound proteins were eluted with 4 × 100 μl of elution buffer (50 mM Tris pH 8, 300 mM NaCl, 5% glycerol, 500 mM imidazole).

The 400 μl NiNTA elutions were incubated with 50 μl of StrepTactin XT Superflow resin for 30 min. The resin was washed with 3 × 1 ml wash buffer (50 mM Tris pH 8, 300 mM NaCl, 5% glycerol, 50 mM imidazole) and bound proteins were eluted with 4 × 50 μl of elution buffer (50 mM Tris pH 8, 150 mM NaCl, 5% glycerol, 50 mM biotin).

Pol α-primase stimulation assays

The assays were performed exactly as described in (11) using poly-dT template, unlabeled ATP, α-^{32}P-dATP, 2 nM primase-Pol α, and the indicated concentrations of CST or ST.

Mass photometry

Purified aliquots of $Cdc13_{OB23}$, $Cdc13_{OB24}$ and $Cdc13_{OB34}$ were thawed and diluted in filtered PBS to a final concentration of 30 nM immediately before mass photometry analysis. All the measurements were performed in a final volume of 20 μl in a Refeyn TwoMP (Refeyn Ltd) calibrated using BSA, γ-globulin and thyroglobulin. Three independent measurements consisting of 1-min movies (1 frame/s) were recorded using the AcquireMP software (Refeyn Ltd) for each protein construct. Analysis of each independent replicate was performed using the DiscoverMP software (Refeyn Ltd).

Size-exclusion chromatography coupled to light scattering (SEC-MALS)

Aliquots of purified OB2 at 0.65 mg/ml and OB4 at 0.3 mg/ml were thawed immediately before SEC-MALS experiments. Both proteins were incubated together in a 1:1 molar ratio for 1 h before the analysis of their interaction. 500 μl of purified protein was fractionated on a Superdex 75 10/300 Increase GL column equilibrated in SEC buffer (25 mM Tris pH 7.5, 150 mM NaCl, 0.5 mM DTT) using an AKTA purifier (GE-Healthcare). The eluted samples were characterized by in-line measurement of the refractive index and multi-angle light scattering using Optilab T-rEX and DAWN 8 + instruments, respectively (Wyatt Technology). Data were analyzed with the ASTRA 6 software and plotted using GraphPad Prism 9.

Analytical ultracentrifugation (AUC)

Protein samples in PBS or 50 mM Tris–HCl pH8.5, 50 mM NaCl and 1 mM EDTA were loaded (320 μl) into 12 mm Epon-charcoal standard double-sector centerpieces and centrifuged in a XL-A analytical ultracentrifuge (Beckman-Coulter Inc.) equipped with UV-VIS absorbance detection system, using an An-50Ti rotor. Sedimentation velocity assays were performed at 48 000 rpm (167 700 g), or 35 000 rpm (89 200 g) for the CST fractions, and sedimentation profiles were recorded by absorbance at 280 or 235 nm, depending on protein concentration. Differential sedimentation coefficient distributions were calculated by least-squares boundary modelling of sedimentation velocity data using the continuous distribution $c(s)$ Lamm equation model as implemented by SEDFIT (37). When necessary, optimization of frictional ratio values was achieved using the continuous $c(s)$ bi-modal f/f_0 Lamm equation model in SEDFIT. These experimental values were corrected to standard conditions using the program SEDNTERP (38) to get the corresponding standard s values ($s20,w$). To estimate the M_w of the proteins and complexes, the partial specific volume was calculated from their amino acid sequence by SEDNTERP (38).

Electrophoretic mobility shift assay (EMSA)

The DNA substrates (Integrated DNA Technologies) (Supplementary Table S1) were resuspended in binding buffer (50 mM Tris–HCl pH 8, 50 mM NaCl, 10% (v/v) glycerol) and incubated with and without the different purified proteins at the indicated concentrations in a final volume of 10 μl. After gentle mixing, samples were incubated for 30 min at 4°C and then loaded onto a 0.4× TBE, 0.7% agarose gel. Electrophoresis was carried out in 0.4× TBE at 100 V and 4°C for 90 min. Finally, the gel was either stained with GelRed (Biotium), washed in 0.4× TBE and imaged with UV illumination or directly imaged in a Typhoon Variable Mode Imager (Amersham Biosciences) using a 480-nm laser and recording the emission at 520 nm for the 6FAM-labeled substrates. Gels were then stained with Quick Coomassie Stain (Protein Ark) for visualization of protein bands.

Fluorescence polarization binding analysis

Binding reactions were set in independent wells of 384-well black plates (Corning Inc., Cat#4511). $Cdc13_{OB234}$, $Cdc13_{OB23}$, $Cdc13_{OB34}$ and OB3 at concentrations ranging from 5 to 0.3 nM were incubated in the dark with 5 nM of 6FAM-labelled 48-mer *Cg*Telo ssDNA substrates for 30 min at 25°C in a final volume of 10 μl. Both DNA and proteins were diluted in 50 mM Tris–HCl pH 7, 50 mM KCl. Fluorescence polarization was measured using a ClarioStar Plus reader (BMG Labtech). K_d values were calculated by non-linear least square fitting of the experimental data to the following equation,

$$Y = \frac{B_{max} * X}{K_d + X}$$

where Y is the average ($n = 3$) of the normalized fluorescence polarization, B_{max} is the maximum polarization observed and X is the protein concentration using Prism9 (GraphPad).

DNA substrate production for magnetic tweezers experiments

We first produced a plasmid named as 56F.pNLrep-Glabrata telomerex10 that contains 10 copies of the telomeric sequence of *C. glabrata* (TGTGGGGTCTGGGTGC) separated by BbvCI restriction sites as follows. We annealed two 5′-phosphorylated oligonucleotides (see Supplementary Table S1) containing two copies of the telomeric sequence of *C. glabrata.* The oligonucleotides were annealed by heating at 95°C for 5 min and cooling down to 20°C at a -1°C min^{-1} rate in hybridization buffer (10 mM Tris–HCl pH 8.0, 1 mM EDTA, 200 mM NaCl and 5 mM $MgCl_2$). Oligonucleotides were designed to create a BbvCI restriction site at both ends after hybridization. The pNLrep plasmid (kindly gifted by Prof. Dr Ralf Seidel) was digested with BbvCI (NEB), purified (QIAGEN) and ligated with this pair of hybridized oligonucleotides rendering a collection of plasmids with different number of copies of the telomeric sequence of *C. glabrata.*

Plasmids were cloned in DH5α Competent cells (Thermo Fisher Scientific), and putative positive colonies with different number of copies of the telomeric sequence selected by colony PCR. Plasmids were purified from cultures using QIAprep Spin Miniprep Kit (QIAGEN), analyzed by restriction digestion, and checked by DNA sequence analysis.

A ssDNA substrate for magnetic tweezers experiments was prepared as follows (39). First, a dsDNA 5326 bp DNA fragment (see Supplementary Table S2 for sequence) was produced by PCR using as a template the plasmid 56F.pNLrep-Glabrata telomerex10 described above, and primers *192.F 93 glabrata* and *193.R 93 biotin* that was 5′ biotinylated (see Supplementary Table S1 for sequences). After purification (QIAGEN), the non-biotinylated end of the PCR fragment was digested with NotI (NEB) and gel purified (QIAGEN). The NotI end was further ligated to a digoxigenin (DIG)-labelled dsDNA fragment, used for immobilization of the DNA molecules. The DIG-labelled handle was prepared by PCR (see Supplementary Table S1 for sequences) including 200 μM final concentration of each dNTP (G,C,T,A) and 10 μM Dig-11-dUTP (all from Roche) using plasmid pSP73-JY0 (40) as template, followed by restriction digestion with NotI. Sample was ready to produce ssDNA (see below) without further purification. DNAs were never exposed to intercalating dyes or UV radiation during their production and were stored at 4°C.

To produce ssDNA molecules for MT experiments we followed the protocol described in (39) with some modifications. In brief, the dsDNA construct with a single biotin in one end and a DIG-labelled handle was incubated with superparamagnetic 2.8 μm streptavidin-coated beads (Dynabeads, Myone Streptavidin, Invitrogen, Carlsbad, CA) for 10 min at room temperature. Then, dsDNA molecules were denatured by addition of 20 μl 0.1 M NaOH (1% BSA) for 15 min at room temperature, producing a biotinylated single DNA strand bound to the magnetic beads that was

separated from the non-biotinylated complementary strand with an external magnet. Note that because the DIG handle contains labelled nucleotides in both strands, the strand bound to the beads will also contain a tail of multiple DIGs. The pellet of beads bound to ssDNA was washed with 20 μl 0.1 M NaOH (1% BSA) to remove remaining free ssDNA strands, and the supernatant discarded again. Magnetic beads were re-suspended in PBS (2% BSA), and deposited in a double PARAFILM (Sigma)-layer flow cell with one cover glass functionalized with anti-DIG antibodies and passivated with PBS (2% BSA). After the adsorption of the beads, we applied a force of 10 pN to remove the non-attached beads and washed with buffer (20 mM Tris–HCl pH 7.5, 30 mM NaCl and 4 mM $MgCl_2$) to clean the fluidic chamber. Tethers of ssDNA with the proper DNA extension at high force were selected for the experiments.

Magnetic tweezers experiments

MT assays were performed using a custom-built MT setup similar to a system previously described (41–44). Briefly, optical images of micrometer-sized superparamagnetic beads tethered to a glass surface by DNA constructs were acquired using a 100× oil-immersion objective and a CCD camera. Real-time image video-microscopy analysis determined the spatial coordinates of the beads with nm accuracy in the *x*, *y* and *z* directions (41) and a pair of magnets located above the sample allowed the application of stretching forces to the bead-DNA system. Applied forces were quantified from the Brownian excursions of the bead and the extension of the DNA tether (44). Data were acquired at 120 Hz to minimize sampling artefacts in force determination. We used vertically aligned magnets coupled to an iron holder to achieve a force of up to 37 pN.

Time courses were obtained by recording the extension of the tether at 4 pN force while 100 nM of Cdc13 in buffer (20 mM Tris–HCl pH 7.5, 30 mM NaCl and 4 mM $MgCl_2$ and 1 mM DTT) was injected into the fluid chamber. An increase in the tether extension by Cdc13 was measured maintaining the force constant until the extension reached a stable maximum plateau. Then, 200 nM of single-stranded DNA molecules containing three copies of the *C. glabrata* telomeric sequence (TGTGGGGT CTGGGTGC) (that we name as *Cg*Telo), or Poly-T ssDNA of the same length were added (see Supplementary Table S1 for sequences used in this work). Changes in tether extension induced by both oligonucleotides were measured using a time window of 40 s in multiple molecules to obtain a mean value for each. All the experiments were carried out at 25°C.

Force-extension data were obtained by measuring the extension of tethers at decreasing forces from 32 to 0.1 pN for a total measuring time of ∼3 min. Force-extension curves were measured on naked ssDNA first. Then, the experiment was repeated on the same molecule at different protein concentrations of full-length Cdc13, individual OB domains or chimeric Cdc13 constructs. This method allowed us to obtain force-extension curves in the absence and presence of protein for each tethered DNA molecule. All the experiments were carried out at 25°C. Data from both time-courses and force-extension curves were analyzed and plotted using Origin Software.

Telomere length analysis

C. glabrata expression plasmids harboring full-length Cdc13 or the $Cdc13_{OB234}$ fragment were constructed by inserting the corresponding fragments (derived from pCDFDuet-H10-TEV-Cdc13 and pCDFDuet-H10-TEV-$Cdc13_{OB234}$) in between EcoRI and SalI sites of the pCN-PDC1 vector (45) which contains the strong PDC1 promoter. The plasmids were transformed into strain BG14 and the transformants selected on YPD supplemented with 50 μg/ml nourseothricin (45).

The transformants were re-streaked once and the resulting colonies used to inoculate liquid cultures. After growth overnight, the cells were harvested and subjected to chromosomal DNA preparations. Southern blot analysis of telomere restriction fragments (TRF Southern) was performed using DNAs treated with EcoRI alone or the combination of EcoRI, MseI, and AluI as previously described (46). The blots were hybridized to an oligonucleotide probe carrying 3 copies of the *C. glabrata* telomere repeat unit (CgTELCx3: $[GCACCCAGACCCCACA]_3$) and analyzed using a PhosphorImager scanner and ImageQuant software. Average telomere lengths for individual TRF clusters were estimated using a previously reported method (47).

Structure prediction and analysis

The structures of OB1 were predicted using the localcolabfold implementation of the AlphaFold2 (AF2) algorithm (48–50). Structural alignments and figure preparation were carried out in ChimeraX (51).

Sequence alignment analysis

Multiple sequence alignment (MSA) was carried out in Clustal Omega with default parameters (52) using Cdc13 orthologs of *C. glabrata* Cdc13 identified by BLAST (53). The representation of residue conservation and the alignment of the secondary structures of *S. cerevisiae* OB1 (PDB: 3WNS) and *C. glabrata* OB1 (AF2 prediction) to the MSA was performed in the ESPript server (54).

RESULTS

Cdc13 assembles as a dimer and larger oligomeric complexes

C. glabrata Cdc13 (Cdc13 hereafter) comprises four OB-fold domains and a small RD domain situated between OB1 and OB2 implicated in the recruitment of telomerase (Figure 1A) (7,55). We cloned Cdc13 containing a TEV-cleavable StrepTrxCL7SUMO or a modified TwinStrep tag fused to the N-terminus for expression in *Escherichia coli* and affinity purification. The protein was then purified using affinity chromatography followed by an anion exchange chromatography step to remove non-specifically bound DNA (Figure 1B). In addition to full-length Cdc13, the purified fraction contained minor degradation products of Cdc13 as determined by mass spectrometry. It has been shown before that Cdc13 enhances the activity of the primase-Pol-α complex when part of the CST complex (11), and we used this property to verify the activity of the recombinantly expressed Cdc13 complex. Stn1 and Ten1 were

co-expressed in *E. coli* BL21 cells and the Stn1-Ten1 complex (ST hereafter) was purified using an N-terminal 10xHis tag in Stn1 that was later removed using the TEV protease (Supplementary Figure S1A). Stn1-Ten1 eluted as a stable, monodisperse complex in SEC (Supplementary Figure S1B) with an apparent molecular weight (MW) consistent with a 1:1 stoichiometry. We also co-expressed Cdc13 together with Stn1 and Ten1 and the resulting CST complex was purified as described for Cdc13 (Supplementary Figure S1A). Cdc13 stimulated the synthesis of RNA-DNA chimera products (from the combined primase and DNA polymerase activity) and displayed a stronger stimulatory effect than Stn1-Ten1 alone (Supplementary Figure S1C, D). This showed that Cdc13 could interact with Stn1-Ten1 and displays functional properties of the Cdc13-Stn1-Ten1 complex, suggesting that the way we produce recombinant Cdc13 preserves at least some of its functionality.

Purified Cdc13 consistently eluted as a major sharp peak at 1.6 ml preceded by a broad peak consistent with high MW species when subjected to size exclusion chromatography (SEC) on a Superose 6 Increase column (Figure 1C). AUC analysis of Cdc13 through the continuous c(s) bimodal f/f0 Lamm equation model showed that the most abundant peak at 6.3S was compatible with a moderately elongated dimer of Cdc13 (see Materials and Methods section for details) (Figure 1D). There were additional peaks that corresponded to molecular species with discreet and incrementally higher sedimentation coefficients (9.6S, 12.4S and 16.4S). This, together with the SEC experiment, indicated that Cdc13 forms not only dimers, but also larger complexes likely formed by the association of 2, 3 and potentially several units of the Cdc13 dimer. These observations reflect the ability of Cdc13 to interact with other Cdc13 molecules to form larger complexes when bound to ssDNA. Whether this is a bona-fide activity, as suggested for *S. cerevisiae* Cdc13 (24,30,34), or a consequence of the recombinant overexpression of the protein is something we cannot fully determine with our experiments (see experiments and discussions below).

Interestingly, the CST complex also eluted as a broad peak in SEC (Supplementary Figure S1B). Several fractions derived from the SEC experiment were then subjected to AUC, revealing a mix of oligomeric species arranged in peaks of increasing sedimentation coefficient (Supplementary Figure S1E). These results suggested that Cdc13 can assemble larger oligomeric species also when complexed with Stn1-Ten1.

Only the OB2 domain behaves as a monodisperse and stable dimer in isolation

We sought to dissect the mechanisms driving Cdc13 oligomerization in *C. glabrata*. For this, we first analyzed the ability of each OB-fold domain in Cdc13 to homo- or hetero-oligomerize. The four individual OB-fold domains were expressed and affinity purified using an N-terminal TwinStrep tag fused for affinity purification (see Methods for details) (Figure 2A). Note that the SDS-PAGE of purified OB4 showed a high MW band that was an aggregation artefact of mixing the protein with standard loading buffer (Figure 2A, indicated with *), since the same sample generated only one band when urea was included in the loading buffer. The oligomeric state of each individual OB-fold domain was determined by SEC in a Superdex 75 column (Figure 2B), MALS and AUC (Supplementary Figure S2). OB3 and OB4 behaved as monomers in SEC, whereas OB2 eluted as a dimer (Figure 2B), and these results were confirmed by SEC-MALS and AUC analysis (Figure 2C, Supplementary Figure S2A). The SEC elution profile of OB1 showed three different peaks (Figure 2B), corresponding to monomers and dimers but also larger species (see next section).

We also analyzed all possible pairwise interactions between the OB domains by AUC to gain further insights into their role in the oligomerization of Cdc13. Only the OB2 and OB4 domains formed a complex in our experimental conditions as assayed by SEC and AUC (Supplementary Figure S2). These results indicate that OB2 and OB4 can interact with each other.

OB1 domain mediates high-order multimerization of Cdc13

In contrast to the well-defined peaks obtained for OB-fold domains 2, 3 and 4 in SEC, Cdc13 OB1 domain resulted in 3 peaks in a Superdex 75 column (~70–3 kDa resolution range), indicating the presence of several oligomeric states (Figure 2B). We injected the same sample in a Superdex 200 column, which resolves species between ~600 and ~10 kDa. This analysis revealed three monodisperse peaks as well as a broad high-MW peak (Figure 2D). All these peaks contain homogeneous OB1 as judged by SDS-PAGE (Figure 2E). AUC of OB1 confirmed it forms several species with increasingly higher MW (Figure 2C). Our results underscore the ability of OB1 to multimerize and form species with a greater number of subunits.

The OB1's propensity to self-associate suggested that this domain could be responsible for the formation of the larger oligomeric species that we observed for Cdc13 (Figure 1C). To test this idea, we prepared four constructs, each of which lacks one individual OB-fold domain (Figure 3A). Curiously, whereas $Cdc13_{OB234}$ was purified as a single band in SDS-PAGE (Figure 3B), all other constructs containing OB1 were difficult to express and produced with a high degree of purity, and they contained a 17 kDa contaminant identified as the *E. coli* protein AccB. Still, the non-truncated versions of $Cdc13_{OB134}$, $Cdc13_{OB124}$ and $Cdc3_{OB123}$ are the more abundant species in these preparations, and the presence of AccB does not likely interfere in our subsequent experiments.

The three constructs containing the OB1 domain, $Cdc13_{OB134}$, $Cdc13_{OB124}$ and $Cdc3_{OB123}$, form high-order species detected as a broad high MW peak in a Superose 6 SEC column (Figure 3C). This behavior is similar to that observed for full-length Cdc13, and it can be explained by the propensity of OB1 to oligomerize. In contrast, the elution profile of $Cdc13_{OB234}$ showed a monodisperse peak in SEC (Figure 3C) and 5.3S in AUC with an estimated MW of 110 kDa (Figure 3D). This is consistent with $Cdc13_{OB234}$ forming a homodimer in solution, given the predicted MW of 57 kDa for a $Cdc13_{OB234}$ monomer. These results strongly support that the minimum structural unit of Cdc13 in *C. glabrata* is a dimer that does not require OB1 for homodimerization, and that can associate into higher-order structures through OB1.

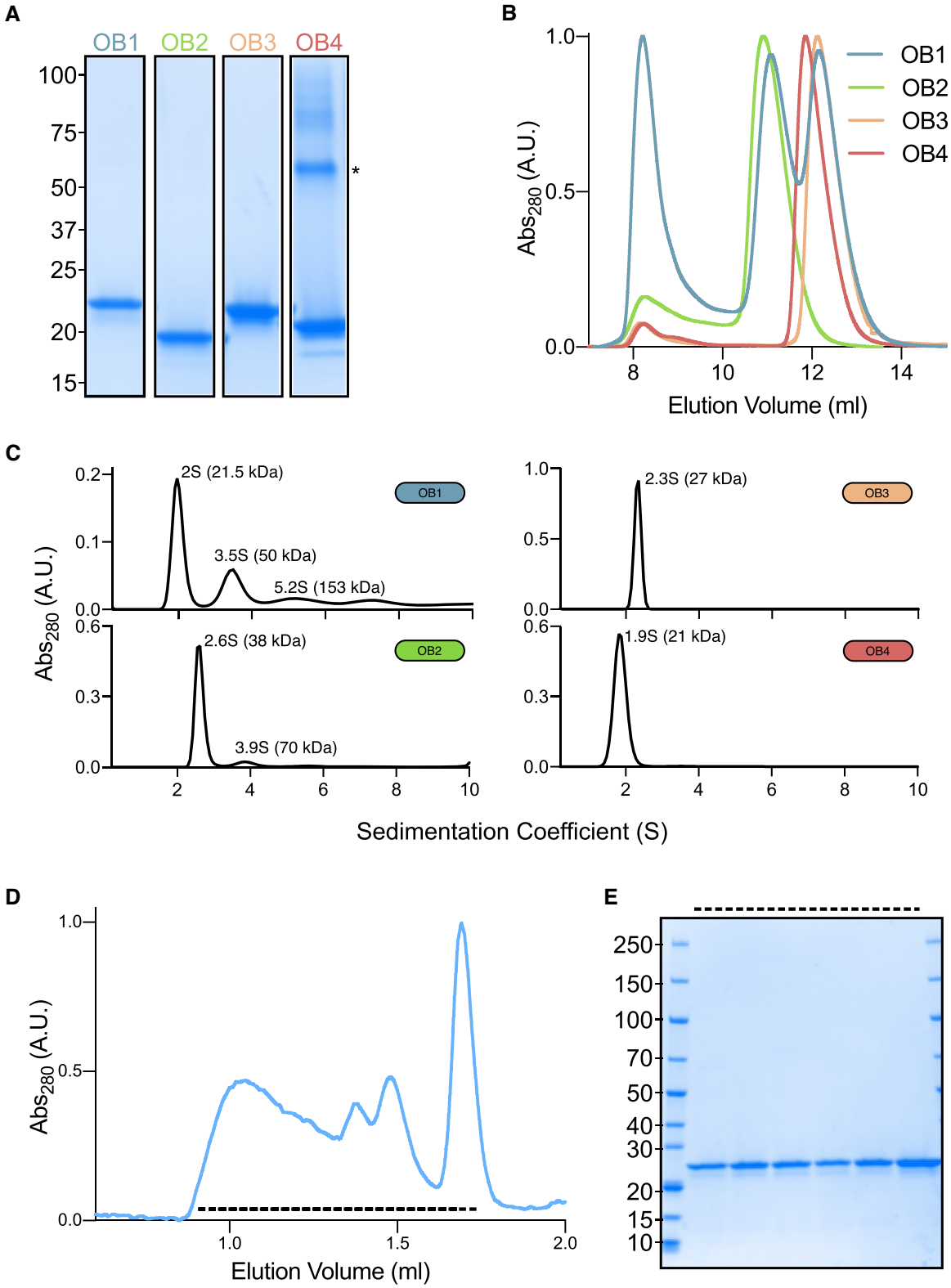

Figure 2. Oligomerization of isolated OB-fold domains in *C. glabrata* Cdc13. (**A**) SDS-PAGE analysis of the purification of each OB-fold domain. * Indicates a high MW band observed in the purified OB4 which is an artifact caused by mixing the protein with SDS-PAGE loading buffer, as the same sample results in only one band of the expected mobility when mixed with urea. (**B**) Superdex 75 Increase SEC profiles of individually purified OB-fold domains. (**C**) AUC analysis of individual OB folds. (**D**) SEC analysis of OB1 in a Superdex 200 3.2/300 column; dotted line indicates the fractions analyzed by SDS-PAGE in panel E. (**E**) SDS-PAGE analysis of all major peaks from OB1 SEC in panel 'D', demonstrating compositional homogeneity.

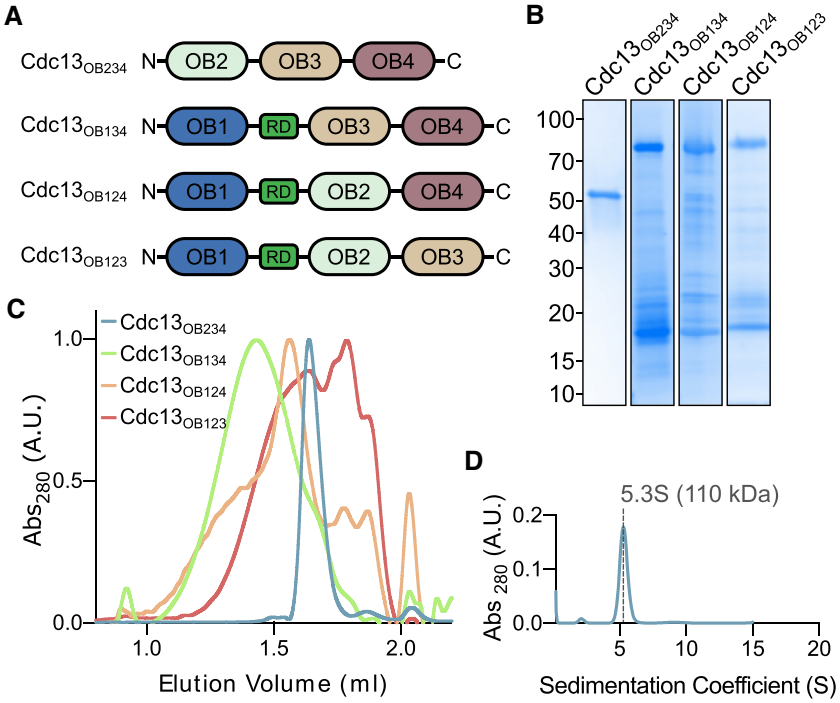

Figure 3. *C. glabrata* Cdc13 is a dimer in solution after removal of OB1. (**A**) Schematic diagram of Cdc13 deletion constructs used. (**B**) SDS-PAGE analysis of the purification of each Cdc13 deletion construct. (**C**) Superose 6 Increase SEC profile of Cdc13 deletion constructs. (**D**) Sedimentation coefficient distribution $c(s)$ profiles of $Cdc13_{OB234}$ showing its dimerization in solution.

Over-expression of Cdc13 lacking OB1 induces telomere shortening in *C.glabrata*

In *S. cerevisiae*, the formation of OB1 domain dimers was shown to regulate telomeric length (24). Our biochemical analyses suggest that the OB1 domain of *C. glabrata* Cdc13 may regulate its oligomerization state. Thus, we asked if the OB1 domain of *C. glabrata* plays a role in telomere regulation, too. We assessed the effect of over-expressing either full-length Cdc13 or $Cdc13_{OB234}$ on telomere lengths *in vivo*. Telomere terminal restriction fragments were generated using either EcoRI alone or EcoRI in combination with MseI and AluI (Figure 4A and B, respectively), and the resulting patterns were similar to those in a previous study (46). Notably, while there were clonal variations, the overexpression of Cdc13 had minimal effects on the lengths of the great majority of telomere restriction fragments when compared to the parental clones and the ones carrying the empty pCN-PDC1 vector. In contrast, the overexpression of $Cdc13_{OB234}$ caused a moderate shortening of telomeres (∼100–150 bp), which were most evident in the case of short telomere clusters (TRF-a, b, c and d) (Figure 4A, B). This observation is consistent with a previous analysis of *Sc*Cdc13, which suggests that disrupting OB1 dimerization can cause a modest reduction in telomere lengths (10).

Mapping OB1 oligomerization interfaces

We then searched for regions responsible for OB1 oligomerization. For this, we performed a systematic mutational analysis to disrupt OB1 oligomerization. A structural prediction of the OB1 domain performed using AF2 (50) revealed a canonical OB domain predicted with high confidence but that contains an apparently disordered C-terminal tail, whose structure cannot be well predicted (Figure 4C, Supplementary Figure S3A, B). This tail is also present and conserved in other Cdc13 orthologs (Supplementary Figure S3C). We first expressed and produced a truncated version of OB1 ($OB1_{\Delta C\text{-ter}}$) without the C-terminal tail (residues 156 to 176) (Figure 1A). Then, we compared its oligomerization state with full-length OB1 using AUC. AUC identified several oligomeric species for OB1 (Figure 4D). Around 72% of OB1 was a monomer, followed by a mix of dimers and other relatively larger oligomeric species (Figure 4D), in agreement with the SEC experiment (Figure 2D). Interestingly, whereas $OB1_{\Delta C\text{-ter}}$ can still form some oligomers, removal of the C-terminal tail significantly reduced the formation of larger species (Figure 4D), suggesting this region is in part responsible for the tendency of OB1 to form higher-order species.

We then searched for possible mutants that could further disrupt oligomerization of $OB1_{\Delta C\text{-ter}}$. Mutants were designed based on oligomerization interfaces found in the crystal structure of OB1 dimers from *S. cerevisiae* (PDB 3NWS) (24) as well as interactions suggested by AF-multimer (49). After an intensive mutagenesis analysis, we identified several mutants that completely abrogated oligomerization, behaving as 100% monomeric in AUC experiments (Table 1). These included R41A, E46A, F88A and K96A (Figure 4C, Supplementary Figure S3D). Mutations in other residues, such as Q39A, A40W and D94A, also reduced the number of oligomeric species in $OB1_{\Delta C\text{-ter}}$, although not completely. Most of these mutants mapped at the regions homologous to the αB helix and β5 strand in *S. cerevisiae*'s OB1, which have been reported to drive

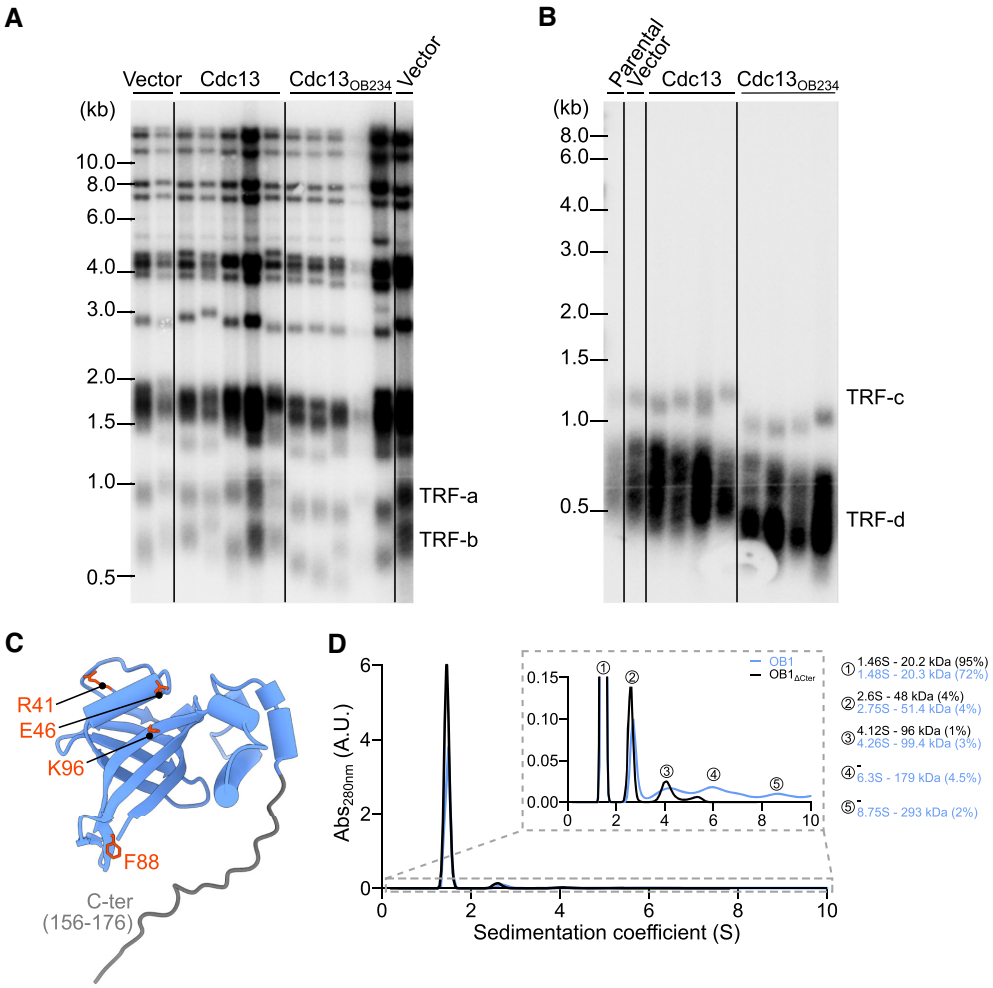

Figure 4. Functional and mutational analysis of *C. glabrata* OB1 domain. (**A**) Southern blot analysis of telomere restriction fragments (TRF) of clones carrying the pCN-PDC1 overexpression vector either empty or containing Cdc13 or $Cdc13_{OB234}$. Chromosomal DNAs were prepared from individual *C. glabrata* clones. The DNAs were digested with EcoRI to release the TRFs and probed with oligos containing three tandem repeats of the *C. glabrata* telomeric sequence. (**B**) Same as A except that DNAs were digested with a combination of EcoRI, MseI, and AluI. (**C**) Predicted structure of the OB1 domain from *C. glabrata* using AF2 (50). Residues mutated are mapped and to the structure. (**D**) AUC analysis of OB1 and $OB1_{\Delta C\text{-ter}}$ oligomerization.

dimerization (24) (Figure 4C, Supplementary Figure S3C). This suggests that this is one of the regions used by OB1 to oligomerize in *C. glabrata*.

Taken together, these results show that OB1 can assemble dimers and larger oligomers using interfaces located at the C-terminal tail of OB1 (residues 156 to 176) and at other interaction surfaces in homologous OB-fold domains.

The OB2 domain mediates dimerization of Cdc13

Our experiments show that *C. glabrata* Cdc13 is a dimer and that when analyzing individual OB-fold domains, only OB2 can assemble into monodisperse and stable dimers. Therefore, we performed additional experiments to determine whether OB2 dimerization is solely responsible for Cdc13 dimerization or other domains also contribute. For this, we generated constructs expressing all three possible combinations of OB pairs but excluding OB1 (i.e. $Cdc13_{OB23}$, $Cdc13_{OB24}$ and $Cdc13_{OB34}$) to avoid the multimerization that hampers analysis of the oligomerization states (Figure 5A). A GGSS sequence was introduced between OB2 and OB4 as a flexible linker in $Cdc13_{OB24}$. These constructs were expressed with an N-terminal TEV-cleavable 10xHis tag for affinity purification (Figure 5B). SEC, AUC and mass photometry experiments showed that constructs containing OB2 ($Cdc13_{OB23}$ and $Cdc13_{OB24}$) behaved as dimers (Figure 5C, Supplementary Figure S4). In contrast, $Cdc13_{OB34}$ was mainly monomeric. This, together with the ability of OB2 to dimerize on its own (Figure 2), further reinforced the role of OB2 as the main driving force for Cdc13 dimerization.

To assess a potential role for OB4 in dimerization—as previously suggested in the literature (22)—we also analyzed if $Cdc13_{OB23}$, $Cdc13_{OB24}$ and $Cdc13_{OB34}$ were able to efficiently dimerize with $Cdc13_{OB234}$, a construct of Cdc13 where we removed OB1 and the RD domain to prevent high-order multimerization. For this, $Cdc13_{OB234}$ fused to an N-terminal StrepTrxCL7SUMO tag was co-expressed with 10xHis tagged versions of either $Cdc13_{OB23}$, $Cdc13_{OB24}$ or $Cdc13_{OB34}$ in *E. coli*. Formation of heterodimers was probed by sequential Ni-NTA and StrepTactin affinity

Table 1. Mutational analyses of OB1

	Most abundant species (sedimentation coefficient, relative abundance)				
	1	2	3	4	5
OB1	1.48S (72%)	2.75S (4%)	4.26S (3%)	6.3S (4.5%)	8.75S (2%)
$OB1_{\Delta C\text{-ter}}$	1.46S (95%)	2.6% (4%)	4.26% (1%)	-	-
$OB1_{\Delta C\text{-ter}}$ + Q39A	1.5S (95.8%)	2.6S (3.1%9)	4.4S (1.1%)	-	-
$OB1_{\Delta C\text{-ter}}$ + A40W	1.5S (97.9%)	2.8S (2.1%)	-	-	-
$OB1_{\Delta C\text{-ter}}$ + R41A	1.5S (100%)	-	-	-	-
$OB1_{\Delta C\text{-ter}}$ + E46A	1.5S (100%)	-	-	-	-
$OB1_{\Delta C\text{-ter}}$ + F88A	1.5S (100%)	-	-	-	-
$OB1_{\Delta C\text{-ter}}$ + K96A	1.4S (100%)	-	-	-	-
$OB1_{\Delta C\text{-ter}}$ + Q39A + A40W	1.5S (97.8%)	3.1S (2.2%)	-	-	-
$OB1_{\Delta C\text{-ter}}$ + A40W + D94A	1.5S (97%)	2.8S (3%)	-	-	-

Table summarizing the oligomerization state of several mutations performed on $OB1_{\Delta C\text{-ter}}$ identified by AUC.

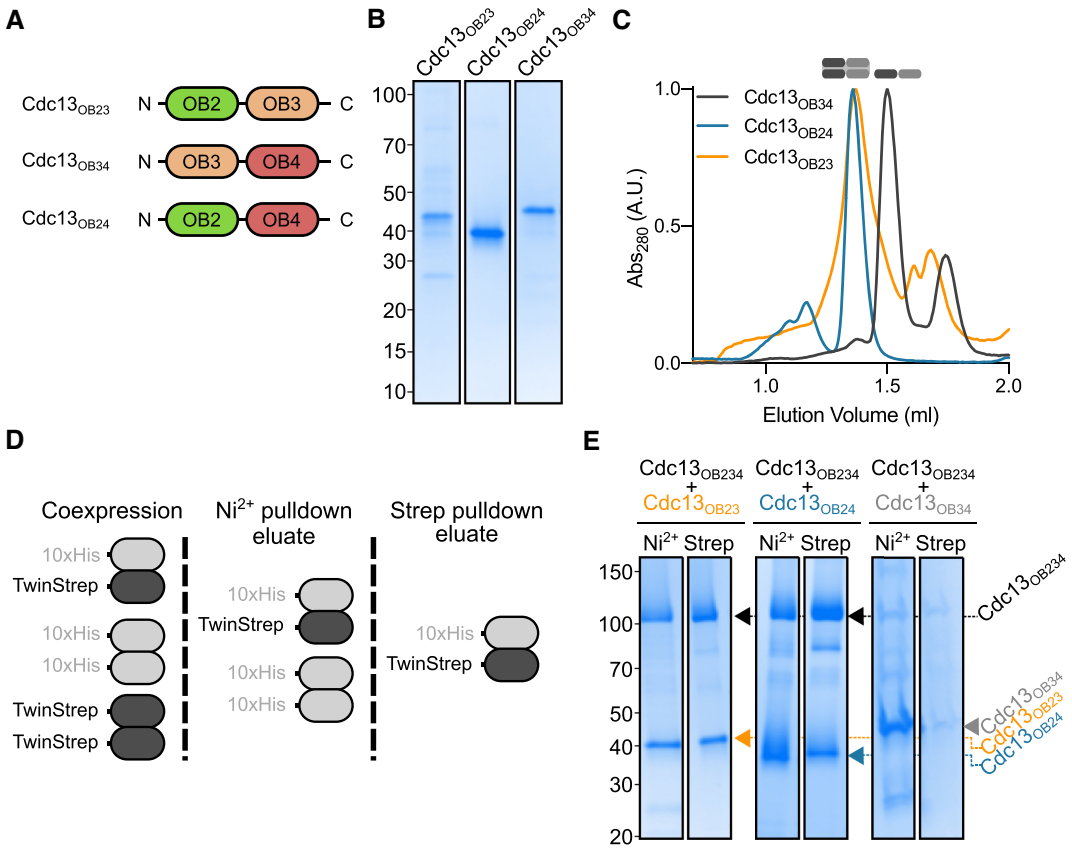

Figure 5. OB2 is the only domain strictly required for dimerization of *C. glabrata* Cdc13. (**A**) Schematic diagram of the Cdc13 double deletion constructs used. (**B**) SDS-PAGE analysis of the purification of each Cdc13 double deletion construct. (**C**) Superdex 200 Increase SEC profile of Cdc13 double deletion constructs. The diagrams indicate the elution peaks of dimers and monomers. (**D**) Diagram summarizing the double pulldown experiment whose results are shown in 'E'. TwinStrep-tagged $Cdc13_{OB234}$ and 10xHis-tagged Cdc13 double deletion constructs were co-expressed in *E. coli*. After lysis, His-tagged Cdc13 double deletion constructs were pulled down by Ni^{2+}-NTA affinity chromatography. From this pool, complexes also containing TwinStrep-tagged $Cdc13_{OB234}$ were pulled down, obtaining only complexes containing both tags. (**E**) SDS-PAGE analysis of the eluates from the double pulldown described in panel D for coexpressions of $Cdc13_{OB234}$ and each of the Cdc13 double deletion constructs. Only $Cdc13_{OB34}$ fails to interact with $Cdc13_{OB234}$.

chromatography (Figure 5D). $Cdc13_{OB23}$, $Cdc13_{OB24}$ were able to pull down $Cdc13_{OB234}$ whilst $Cdc13_{OB34}$ was not (Figure 5E). Therefore, neither two OB4 domains or one OB2 together with two OB4s are able to drive dimerization. These results indicate that *C. glabrata* Cdc13 forms dimers requiring only the contribution of one OB2 domain from each of the monomers. We cannot rule out that OB1 also dimerizes in the context of the Cdc13 dimer, but clearly the OB2 domain is sufficient for dimerization.

Cdc13 unfolds secondary structure in *C.glabrata* telomeric repeats

How Cdc13 binds telomeric DNA, how Cdc13 affects the structure of telomeric DNA, and the contribution of each domain and oligomerization to DNA binding are still poorly characterized. Therefore, we sought to investigate how each individual OB-fold domain and the oligomerization of Cdc13 in *C. glabrata* affect its DNA binding activity.

First, we investigated the binding of Cdc13 to ssDNA using magnetic tweezers (MT) (56,57). This set-up monitors the extension of individual DNA tethers subjected to a force applied by a pair of magnets. Duplex DNA molecules containing 10 copies of *C. glabrata* telomeric repeats and labeled on one end with a single biotin and with a multi-labelled digoxigenin handle on the other end were prepared as described in methods. Duplex DNA molecules were then denatured and the biotinylated strand immobilized between a glass surface and super-paramagnetic streptavidin-coated beads (Supplementary Figure S5A). ssDNA molecules were easily identified because at 4 pN, ssDNA folds into secondary structures resulting in a compacted form with an extension of ∼0.4 μm, much lower than the extension of duplex dsDNA (Supplementary Figure S5B). Using MT, we measured the extension of ssDNA tethers following injection of full-length Cdc13 and different Cdc13 truncation variants (Figure 6A). Upon injection of 100 nM full-length Cdc13, the extension gradually increased up to ∼1 μm (Figure 6B, i). We interpreted this result as the unfolding of secondary structures by the binding of Cdc13, as a similar effect was observed using other ssDNA binding proteins (41,58). Importantly, the extended state remained unaltered upon further injection of only buffer after Cdc13 binding, suggesting a stable protein–DNA interaction (Figure 6B, i). To confirm that this unfolding effect was caused by the binding of Cdc13 to the DNA, we injected oligonucleotides containing three repeats of *C. glabrata*'s telomeric sequence (*Cg*Telo, corresponding to a 48mer) to compete for the protein bound to the DNA and monitored the extension of the DNA molecule. Indeed, the addition of *Cg*Telo to the extended *Cg*Cdc13–ssDNA complex induced a fast and marked reduction of the DNA extension (Figure 6B, ii). In contrast, addition of an oligonucleotide containing a polyT sequence of the same length (polyT) produced a smaller and more gradual reduction in the extension of the DNA (Figure 6B, iii). Quantification of the relative decrease of the extension of the DNA molecule showed that while the polyT oligonucleotide produced a 10% decrease, the decrease was roughly 50% in the case of the *Cg*Telo oligo within a 60 s time period (Figure 6C). These results showed that Cdc13 binds specifically to *C. glabrata* telomeric repeats, and this binding results in the unfolding of the secondary structures present in ssDNA.

All domains in Cdc13 are involved in DNA binding and unfolding activity

Next, we compared the binding properties of individual OB domains and Cdc13 constructs by performing force-extension experiments. In these experiments, we mechanically unfolded ssDNA molecules, exposed them to different proteins, and monitored the extension while reducing the force to 0.1 pN. Consistent with our previous result, the binding of Cdc13 to ssDNA prevented ssDNA refolding, resulting in increased extensions of ssDNA tethers (compare bare ssDNA and Cdc13 in Figure 7A). Extensions of bare ssDNA and Cdc13-ssDNA equaled at around 10 pN indicating that at this force the Cdc13 nucleoprotein filament was fully extended. We then investigated the binding of each individual OB domain to *C. glabrata* telomeric sequences. In sharp contrast to full-length Cdc13, none of the isolated OB-fold domains significantly affected the extension of DNA when compared to the bare ssDNA (Figure 7A). We thus tested if any of these individual OB-fold domains could bind to DNA in electrophoretic mobility shift assays (EMSAs). Only OB3 was able to bind to *Cg*Telo (Figure 7B, Supplementary Figure S6A). This result was consistent with the findings in the yeast *S. cerevisiae* and *K. lactis,* both of which use Cdc13 OB3 to bind ssDNA (32,59,60). The *C. glabrata* OB3 did not bind to an unstructured polyT oligonucleotide, but we detected some binding to a 48mer substrate containing 8 repeats of the human telomeric sequence (5′- TTAGGG -3′) (*Hs*Telo); this binding was significantly weaker than the binding to *Cg*Telo (Figure 7B). Together, these results indicate that although OB3 is capable of binding to ssDNA, this domain on its own is not sufficient to prevent the formation of secondary structures in telomeric single-stranded DNA.

Our results raised the possibility that several domains of Cdc13 and/or Cdc13 oligomerization could contribute to the properties of Cdc13 in DNA binding. To explore this hypothesis, we first tested the effect of Cdc13 dimerization in DNA binding using EMSA experiments (Figure 7C, Supplementary Figure S6B). Interestingly, we found significant differences between constructs that contained OB3 but with or without OB2. $Cdc13_{OB234}$ binds to ssDNA as well as full-length Cdc13, and both constructs showed a preference for *C. glabrata* telomeric repeats. Under the conditions tested, $Cdc13_{OB134}$, a construct that lacks only OB2, showed significantly less binding to DNA than Cdc13 or $Cdc13_{OB234,}$ indicating that OB2, the main domain responsible for Cdc13 dimerization, is important for optimal DNA binding (Figure 7C). These experiments showed that under the conditions of EMSA experiments, the presence of OB1 (a domain that oligomerizes on its own) in $Cdc13_{OB134}$ is insufficient to substitute the effect of OB2 in DNA binding. DNA binding was also affected by removal of OB4 in $Cdc13_{OB123}$. To corroborate the EMSA results, we examined the activities of Cdc13 truncation variants using fluorescence polarization binding assays. Using 6FAM labelled *Cg*Telo (6FAM-*Cg*Telo) (Supplementary Table S1) as binding substrate, we estimated the K_d of $Cdc13_{OB234}$, $Cdc13_{OB23}$, $Cdc13_{OB34}$ and OB3 to be around 13, 29, 299 and 488 nM, respectively (Figure 7D), demonstrating that the presence of OB2 significantly enhanced the binding of OB3 to ssDNA, whereas the presence of OB4 improved binding only slightly. These results suggest that Cdc13 dimerization through OB2 is important to promote binding to telomeric sequences and that OB4 contributes more modestly to DNA binding. Since OB4 and OB2 form a complex when incubated together (Supplementary Figure S2), it is possible that the interaction between OB2 and OB4 could also contribute to facilitate OB3 binding to ssDNA and/or maintain the dimeric state.

We then performed force-extension experiments with Cdc13 constructs lacking OB2, the OB-fold domain responsible for dimerization, or OB1, possibly responsible for multimerization (Figure 7E). Control experiments using the $Cdc13_{OB124}$ construct showed extensions comparable to those of bare ssDNA, demonstrating that the observed effects of proteins on DNA extensions were dependent on the

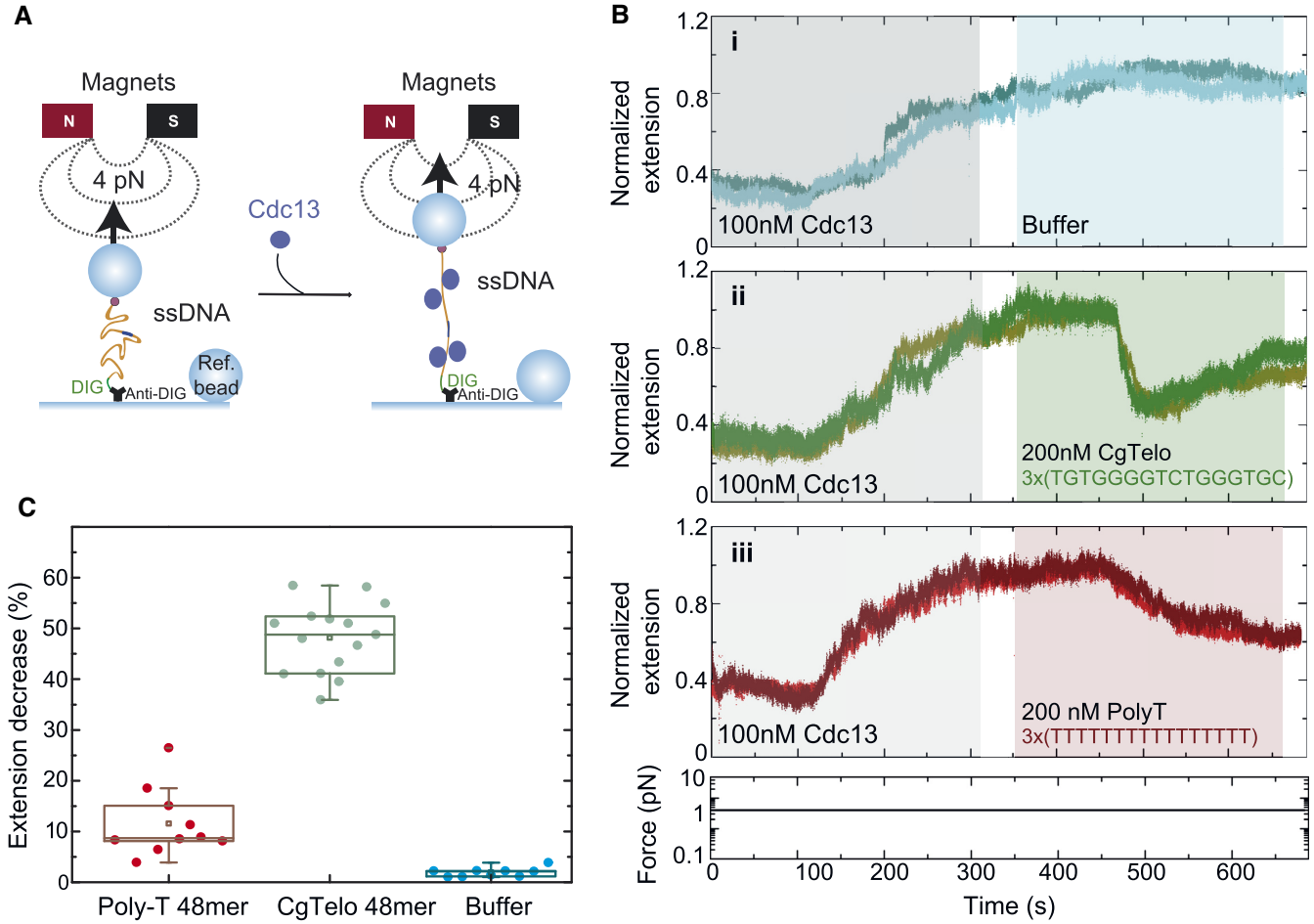

Figure 6. Single-molecule magnetic tweezers experiments to study *C. glabrata* Cdc13 interactions with telomeric sequences. (**A**) Cartoon of the experiment to study Cdc13-ssDNA interactions in magnetic tweezers. (**B**) MT time courses show the increase of extension of ssDNA held at 4 pN upon injection of 100 nM Cdc13, consistent with the unfolding of ssDNA secondary structures. Cdc13 bound to ssDNA is not displaced by the injection of plain buffer (i). A remarkable reduction of DNA extension is observed upon injection of 200 nM specific *C. glabrata* telomeric oligonucleotide (ii). A mild displacement of Cdc13 bound to ssDNA is observed upon injection of 200 nM poly-T oligonucleotide (iii). (**C**) Quantification of 'B', as extension decrease upon injection of buffer ($n = 9$), PolyT oligonucleotide ($n = 10$), and *Cg*Telo oligonucleotide ($n = 15$).

DNA-binding activity of OB3 (Figure 7E). Cdc13 without OB1 or OB2 ($Cdc13_{OB234}$, $Cdc13_{OB134}$, see Figure 3) can still prevent the refolding of ssDNA but not to the same extent as full-length Cdc13 (Figure 7E). Curiously, removal of OB4 ($Cdc13_{OB123}$) also affected this refolding activity. Given that OB4 interacts with OB2, and that OB4 contributes to DNA binding in EMSA and fluorescence polarization experiments, we interpreted this as indication of a structural role for this domain that contributes to Cdc13 dimerization or DNA binding. We also performed force-extension experiments using constructs containing only two OB-fold domains, including $Cdc13_{OB23}$, $Cdc13_{OB24}$ and $Cdc13_{OB34}$ (Figure 7F). As expected, $Cdc13_{OB24}$, which lacks OB3, had no effect on DNA. On the other hand, $Cdc13_{OB23}$ and $Cdc13_{OB34}$, which lack OB1, similarly prevented the refolding of ssDNA but not to the extent of full-length Cdc13 (Figure 7F).

Therefore, although OB3 is the only domain that binds to telomeric sequences by itself, OB2 and OB4 promote binding, suggesting that dimerization and/or the interaction of OB2 and OB4 places OB3 in a more active conformation to bind ssDNA. Cdc13 unfolds the structure of ssDNA and once bound, it prevents its refolding. The OB1 domain in Cdc13 also contributes to maintaining the unfolded structure of ssDNA, suggesting that every domain in Cdc13 is needed to alter the structure of DNA.

Discussion

CST, a central player in telomere homeostasis present in a wide range of organisms, is formed by three proteins, CTC1 (in mammals)/Cdc13 (in yeast), STN1/Stn1 and TEN1/Ten1 (4,6,61,62). Whereas STN1/Stn1 and TEN1/Ten1 are highly conserved from yeast to humans, Cdc13 does not resemble its mammalian counterpart CTC1 either in sequence or domain organization. Also, yeast Cdc13 but not mammalian CTC1 has been shown to perform functions on its own and independently of the other two subunits (25,26). While the structure of human CTC1 has recently been elucidated as part of the CST complex (21,28,29), the information about the architecture and molecular organization of yeast Cdc13 is still fragmentary

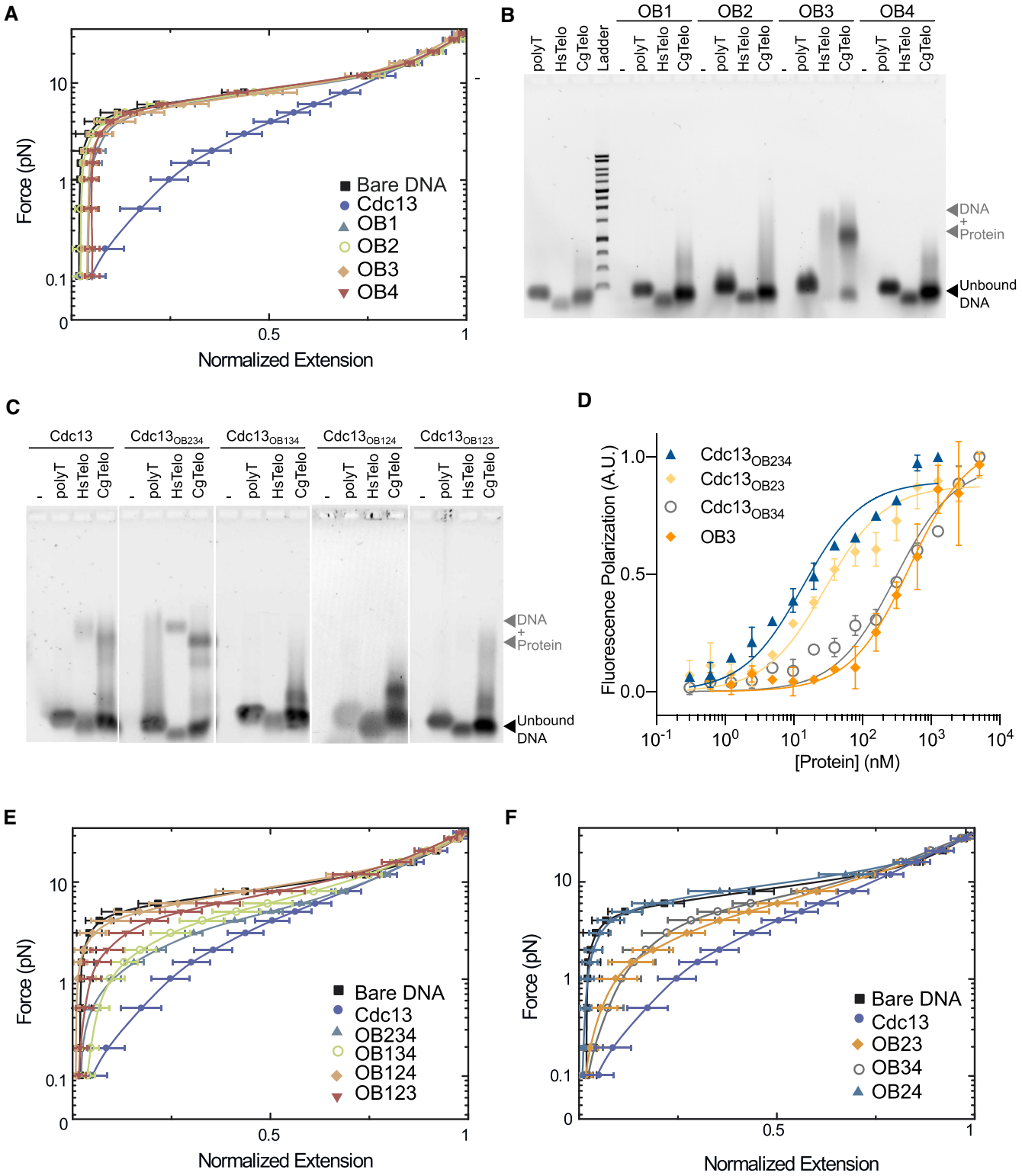

Figure 7. DNA binding properties of individual OB domains and Cdc13 constructs. (**A**) Average magnetic tweezers force-extension curves of ssDNA taken in the presence of Cdc13 ($n = 13$), OB1 ($n = 8$), OB2 ($n = 6$), OB3 ($n = 5$) and OB4 ($n = 4$). (**B**) EMSA analyses in agarose gels of individual OB fold domains. (**C**) EMSA analyses in agarose gels of full-length as well as several truncated versions of Cdc13. (**D**) Fluorescence polarization DNA binding assays of OB3, $Cdc13_{OB34}$, $Cdc13_{OB23}$ and $Cdc13_{OB234}$. Dots represent the normalized average ($n = 3$) and error bars show the standard deviation of each measurement. The single-site binding model equation was fitted to calculate the following K_d ($K_d \pm$ sd): 13.5 ± 1.7 nM ($Cdc13_{OB234}$), 28.5 ± 3.8 nM ($Cdc13_{OB23}$), 299 ± 41 nM ($Cdc13_{OB34}$), 488 ± 90 nM (OB3). (**E**) Average force-extension curves of ssDNA taken in the presence of Cdc13 ($n = 13$), $Cdc13_{OB234}$ ($n = 14$), $Cdc13_{OB134}$ ($n = 12$), $Cdc13_{OB124}$ ($n = 22$) and $Cdc13_{OB123}$ ($n = 15$). (**F**) Average force-extension curves of ssDNA taken in the presence of Cdc13 ($n = 13$), $Cdc13_{OB23}$ ($n = 22$), $Cdc13_{OB34}$ ($n = 15$) and $Cdc13_{OB24}$ ($n = 21$). Data included in A, E and F for bare ssDNA is the average of 25 ssDNA molecules obtained in the absence of protein. Errors are standard deviation of the mean (SD) for measurements performed on different molecules.

and somewhat inconsistent. Available structures for yeast Cdc13 are limited to individual domains or combinations of domains from different species and some contradictory findings have been reported. In addition, the interpretation of *in vivo* experiments, which have made use mostly of *S. cerevisiae* mutants, and the correlation between the mutations performed and the resulting phenotypes is challenging, as illustrated by the studies on Cdc13 homodimerization. Although it is widely accepted that Cdc13 can dimerize and that this oligomeric state is important for its function, it is still unclear how two monomers interact. Three out of the four OB-fold domains that comprise Cdc13 have been reported to form homodimers in isolation, OB1 and OB2 in *S. cerevisiae* (10,23,24) and OB4 in *C. glabrata* (22). In this latter case, OB4 dimerizes using a different interaction surface than the one observed for OB2 in *S. cerevisiae*. OB1 is also apparently responsible for dimerization in *S. cerevisiae* since a single point mutation disrupts dimerization of OB1 and the full-length Cdc13 (31). In *K. lactis,* a crystal structure of a Cdc13 construct lacking OB1 and OB3 shows that Stn1 functions as a bridge connecting OB2 and OB4 from two different monomers, whereas OB2 and OB4 of each monomer interact (32). These disparate results might just reflect experimental differences of a fundamentally conserved architecture for yeast Cdc13, or alternatively, yeast Cdc13 and the CST complex could have evolved to adopt several distinct architectures with Cdc13 assembling differently in different species. To address this question, we have characterized the organization of Cdc13 from *C. glabrata*. We selected this species because it harbors the only yeast CST complex where all three full-length subunits can be expressed and reconstituted through a recombinant system. In addition, while not much is known about its molecular organization, the available evidence suggests it might differ significantly from *S. cerevisiae* (33). We have performed extensive *in vitro* studies that allowed us to propose a model for its architecture and how this influences DNA binding and oligomerization.

C. glabrata Cdc13 dimerizes through its OB2 domain, and this is the only domain strictly essential for the formation of a stable dimer (Figure 8A, B). We cannot rule out that two OB4 domains could also interact between each other in the context of the dimeric Cdc13, since a residual peak compatible with a dimer was also detected in some of our SEC experiments. Moreover, OB4 from *C. glabrata* forms dimers under the high concentration conditions of crystallization studies (22). OB3 is the only domain that binds ssDNA but its DNA-binding property is altered by OB2 and OB4. In particular, OB3 together with either OB2 or OB4 is the minimum combination of domains that prevents refolding of ssDNA in magnetic tweezers assays, and both OB2 and OB4 each enhance the ability of OB3 to efficiently bind ssDNA in EMSA experiments. Since OB2 and OB4 can interact, these results together suggest the formation of a core functional unit of Cdc13 by OB2, OB3 and OB4. Our DNA-binding studies, performed in the context of short ssDNA and EMSA experiments, show that *C. glabrata* Cdc13 has preference for telomeric sequences of this species versus humans, and that whereas only OB3 alone binds to DNA, dimerization through OB2 promotes binding of the OB3 domain to ssDNA and that OB3 cooperates with the other domains to prevent refolding of ssDNA. These results contrast with the DNA-binding studies in *S. cerevisiae* where ssDNA binding affinity is independent of dimerization (31).

Our findings for *C. glabrata* Cdc13 are consistent with the impact of some mutations and deletions described for *S. cerevisiae* and this points to some similarities between both species. The deletion of OB4 in *S. cerevisiae* does not immediately abrogate Cdc13 function *in vivo,* whereas deletion of OB2 or OB3 impairs Cdc13 binding to DNA and cell viability (63). Supporting a central role of OB2 in Cdc13, a point mutation (P371S) in this domain generates the *cdc13-1* ts mutant, which is widely used in *S. cerevisiae* for studying cell cycle arrest and DNA damage checkpoint mechanisms (64). Additionally, OB2 dimerization was essential for the binding of the Stn1-Ten1 complex to *S. cerevisiae* Cdc13 (23). Mutations that disrupt OB2 dimerization in *S. cerevisiae* exhibit growth and telomere length defects *in vivo*, but these do not disrupt DNA binding. Interestingly, these mutants remained as dimers in solution held by interactions between OB1 (23). These results are broadly in agreement with what we have found for *C. glabrata,* except for the contribution of OB2 and OB4 to DNA binding in *C. glabrata*. The fact that Cdc13 is able to form oligomers through OB1 and OB2 domains independently could be responsible for some of the disparate results that have been reported in the literature.

Cdc13 is known to act during telomere replication and under replicative stress where long ssDNA stretches are generated. To analyze the function of the protein in the context of longer ssDNAs we used a magnetic tweezers setup. These experiments showed that Cdc13 binds and unfolds secondary structures in ssDNA, and once bound, Cdc13 prevents its refolding. Interestingly, OB3 alone is not sufficient to prevent refolding (Figure 7) or induce unfolding (not shown) despite being able to bind ssDNA in EMSAs. Moreover, whilst some of this activity is restored when OB3 works together with at least one other domain, full activity was only present in the full-length protein. Removal of OB1, OB2 or OB4 affected the unfolding activity of Cdc13, suggesting that every domain contributes to the ability of Cdc13 to maintain an unfolded structure of ssDNA. The need for OB2 and OB4 could be explained if dimerization is important for Cdc13 to alter the structure of DNA. OB2 is essential for Cdc13 to form dimers, and OB4 interacts with OB2 (Supplementary Figure S2), and removal of OB4 affects DNA binding in EMSA experiments (Figure 7).

In addition to homodimerization, we have observed the formation of higher-order oligomers in *C. glabrata* Cdc13 (Figure 1C). AUC experiments suggest that these larger species are formed by the stepwise interaction of Cdc13 dimers (Figure 1D). In our model system, the multimerization of Cdc13 is clearly linked to the OB1 domain and its removal results in a Cdc13 molecule that behaves as a stable and soluble dimer that binds efficiently to DNA. It might be possible that the oligomerization observed is caused by the recombinant overexpression of the protein. However, we do not consider this scenario very likely, given that we have identified mutations that abrogate the dimerization and oligomerization of OB1 completely (Figure 4C, D) and

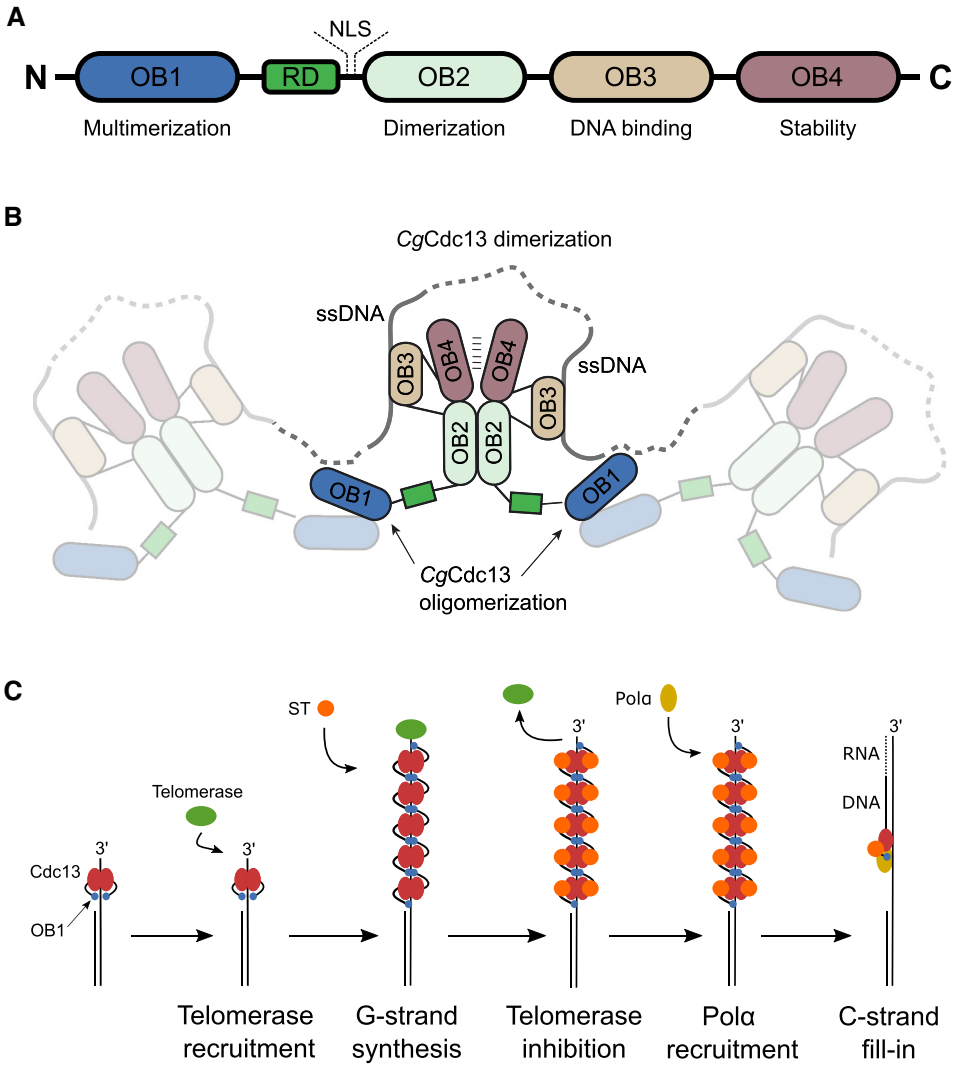

Figure 8. Model for the molecular organization of *C. glabrata* Cdc13. (**A**) Function of each domain in *C. glabrata* Cdc13. (**B**) Model of the interactions and molecular architecture of *C. glabrata* Cdc13. OB2 and OB4 interact to promote DNA binding by OB3. OB2 is responsible for dimerization. OB4 does not dimerize on its own but it interacts with OB2 and potentially dimerize when in the context of the full protein. OB2 and OB4 cooperate to promote DNA binding by OB3. The main function of OB1 is to assembly large order oligomers. (**C**) Speculative model suggesting a protective function of oligomeric *C. glabrata* Cdc13 and CST during telomere maintenance.

we also find that OB1 is needed for regulating telomere extension in *C. glabrata* (Figure 4A-B). Our observations are in agreement with previous reports on the importance of Cdc13 multi/oligomerization. Qian *et al* observed that Cdc13 from *S. cerevisiae* eluted as a complex of a molecular weight of ∼400 kDa in SEC experiments and they proposed that Cdc13 formed an oligomer (34). Mitchell *et al.* (24) and Sun *et al.* (10) found that *S. cerevisiae* OB1 forms dimers, and that these are important for regulating telomeric length (24). Finally, Lin *et al.* found that *S. cerevisiae* Cdc13 can remodel telomeric DNA suggesting the formation of a nucleoprotein complex based on the oligomerization of Cdc13 (30). Our single-molecule experiments show that OB1 is needed for the full maintenance of an unfolded state of ssDNA bound to Cdc13, which would fit a model where OB1 facilitates the oligomerization of Cdc13 on the DNA. Therefore, we suggest that it might be possible that the tendency of OB1 to drive Cdc13 self-association *in vitro* might reflect the mechanism for the formation of a large nucleoprotein complex that affects the structure of ssDNA (Figure 8B). Supporting this idea, cryoEM studies of Replication Protein A (RPA), a ssDNA binding protein complex composed of three subunits (RPA70, RPA32 and RPA14) and whose domain composition is reminiscent of the CST complex, revealed several RPAs forming higher order assemblies on ssDNA that modulate its function (65). Two adjacent RPAs associate on the ssDNA using interactions between specific domains of each molecule. We speculate that similarly to RPA, the association of several Cdc13 molecules on ssDNA would stabilize a conformation of Cdc13 and the telomere that could be important for function.

Despite sharing similar functions in telomere homeostasis, the molecular organization of the CST complex has

diverged significantly between humans and yeast. Moreover, differences found between the *S. cerevisiae*, *C. glabrata* and *K. lactis* complexes in several studies suggest that each species may have evolved different architectures. Thus, the molecular organization of yeast Cdc13 and CST complex remain unclear and the possibility of alternative architectures in different yeasts cannot be discounted. Here, we have systematically dissected the molecular organization and the mechanism of oligomerization of Cdc13 in *C. glabrata*. This Cdc13 forms a dimer where OB2 and OB4 interact to help OB3 acquire a configuration that promotes binding to ssDNA (Figure 8A, B). *C. glabrata* Cdc13 could potentially form large oligomers to remodel the structure of long ssDNA stretches in telomeric DNA. These large complexes also formed in the context of the CST complex, and this might explain why some large oligomeric species were detected in previous studies that were interpreted as an unusual organization of the CST complex. Is then this molecular model unique to *C. glabrata* or applicable to other yeast species? Although we have not performed specific experiments to address this issue, an evaluation of the published data, coupled with our detailed analysis of Cdc13's domains, allows us to propose the evolution of alternative Cdc13 architectures in different yeasts but which nevertheless share common features and organizing principles. One common feature is the utilization of OB2 for Cdc13 dimerization, which is demonstrated in both *S. cerevisiae* (23) and *C. glabrata* (this work). Just like *C. glabrata*, the OB2 and OB4 from *K. lactis* Cdc13 molecule interact (32) (Figure 8B). We propose that this OB2-OB4 interaction organizes a core with OB3, which is responsible for DNA binding in *S. cerevisiae*, *C. glabrata* and *K. lactis*. Finally, the mechanism of multimerization mediated by OB1 in *C. glabrata* may explain some of the discrepancies in the literature as OB1 can sustain the formation of large oligomeric species regardless of other domains such as OB2. Other studies of telomeres have previously suggested that there are far more similarities than differences between systems once all information from various organisms is put into context (63,66). In summary, we propose here a model for the molecular organization of *C. glabrata* Cdc13 and suggest that the core of the interactions and oligomerization mechanisms found in *C. glabrata* will be conserved in other yeast, with some differences such as the function of the OB4 domain or the changes required to recognize specific telomeric sequences.

The domain architecture that we describe in this work (Figure 8B), together with previous structural, biochemical and functional data, can be used to construct an integrated model for the role of Cdc13 in telomere replication (Figure 8C). During the G1 phase, Cdc13 is bound to the telomeric G-overhang (67). Upon progression into late S-phase, the post-translational modifications of the Cdc13 RD domain (26) and the induction of Est1 expression (68) lead to the recruitment of telomerase to the 3′ overhangs of telomeres (69). As the G-strand is elongated, more Cdc13 would be recruited, facilitating the formation of multimers mediated by OB1. The observations that the *S. cerevisiae* OB1 domain displays low affinity for ssDNA binding in an oligomerization dependent way suggest that this domain may also contact DNA following multimerization (23,24). At the end of S-phase, Cdc13 is SUMOylated at the C-terminus of its OB4 domain (55), stabilizing the interaction with the ST complex to form the CST complex that will recruit Pol α (Figure 8C). We hypothesize that the post-translational modification of Cdc13 could induce conformational changes in the complex. It is conceivable that alternative configurations of the CST complex are possible at different stages of the process, maybe some in accordance with what has been proposed for *K. lactis* (32). Moreover, the Cdc13 OB1-Pol α and Cdc13 OB1-ssDNA interactions are known to be mutually exclusive (10,24), suggesting that the interaction with Pol α could lead to a different arrangement of OB1 that favors CST multimer disassembly. In line with this model, the recently reported structures of the human CST-Pol α complex show that only monomeric CST can interact with Pol α (28,29). Effective recruitment of Pol α will allow C-strand fill-in and completion of telomere replication. The ability of Cdc13 to unfold G-strand and prevent refolding may also facilitate the action of Pol α. Our findings underscore the importance of the oligomeric state of Cdc13 and the CST complex, as well as Cdc13-mediated telomeric DNA unfolding in their functions.

DATA AVAILABILITY

All raw data presented in this work is available upon request.

SUPPLEMENTARY DATA

Supplementary Data are available at NAR Online.

ACKNOWLEDGEMENTS

We thank the help of Clara Santiveri and Ramón Campos from the CNIO Spectroscopy and Nuclear Magnetic Resonance Unit for their help in SEC-MALS. We thank Carmen Arroyo, student at CNIO for help in the fluorescence polarization experiments. We thank the help of Jasminka Boskovic and the CNIO EM Unit for help in initial stages of this work. We thank REFEYN (Oxford, UK) for their assistance during mass photometry measurements.

FUNDING

Agencia Estatal de Investigación [AEI/10.13039/501100011 033]; Ministerio de Ciencia e Innovación, and co-funded by the European Regional Development Fund (ERDF-UE) [PID2020-114429RB-I00 to O.L., PID2020-112998GB-100 to F.M.-H]; Autonomous Region of Madrid and co-funded by the European Social Fund and the European Regional Development Fund [Y2018/BIO4747 and P2018/NMT4443 to O.L. and F.M.-H.]; National Institute of Health Carlos III to CNIO; J.R.L.O. and O.N. acknowledge support from the Molecular Interactions Facility at the CIB-CSIC; N.G.-R. was supported by a Boehringer Ingelheim Fonds PhD fellowship; N.F.L. is funded by NIH [GM107287]. Funding for open access charge: Agencia Estatal de Investigación [AEI/10.13039/501100011 033]; Ministerio de Ciencia e Innovación, co-funded by the European Regional Development Fund (ERDF) [PID2020-114429RB-I00].

Conflict of interest statement. None declared.

REFERENCES

1. de Lange,T. (2009) How telomeres solve the end-protection problem. *Science*, **326**, 948–952.
2. Soudet,J., Jolivet,P. and Teixeira,M.T. (2014) Elucidation of the DNA end-replication problem in *Saccharomyces cerevisiae*. *Mol. Cell*, **53**, 954–964.
3. Lim,C.J. and Cech,T.R. (2021) Shaping human telomeres: from shelterin and CST complexes to telomeric chromatin organization. *Nat. Rev. Mol. Cell Biol.*, **22**, 283–298.
4. Lue,N.F. (2018) Evolving linear chromosomes and telomeres: a C-strand-centric view. *Trends Biochem. Sci*, **43**, 314–326.
5. Giraud-Panis,M.J., Teixeira,M.T., Géli,V. and Gilson,E. (2010) CST meets shelterin to keep telomeres in check. *Mol. Cell*, **39**, 665–676.
6. Price,C.M., Boltz,K.A., Chaiken,M.F., Stewart,J.A., Beilstein,M.A. and Shippen,D.E. (2010) Evolution of CST function in telomere maintenance. *Cell Cycle*, **9**, 3157–3165.
7. Evans,S.K. and Lundblad,V. (1999) Est1 and Cdc13 as comediators of telomerase access. *Science*, **286**, 117–120.
8. Wu,Y. and Zakian,V.A. (2011) The telomeric Cdc13 protein interacts directly with the telomerase subunit Est1 to bring it to telomeric DNA ends in vitro. *Proc. Natl. Acad. Sci. U.S.A.*, **108**, 20362–20369.
9. Qi,H. and Zakian,V.A. (2000) The Saccharomyces telomere-binding protein Cdc13p interacts with both the catalytic subunit of DNA polymerase alpha and the telomerase-associated est1 protein. *Genes Dev.*, **14**, 1777–1788.
10. Sun,J., Yang,Y., Wan,K., Mao,N., Yu,T.Y., Lin,Y.C., DeZwaan,D.C., Freeman,B.C., Lin,J.J., Lue,N.F. *et al.* (2011) Structural bases of dimerization of yeast telomere protein Cdc13 and its interaction with the catalytic subunit of DNA polymerase α. *Cell Res.*, **21**, 258–274.
11. Lue,N.F., Chan,J., Wright,W.E. and Hurwitz,J. (2014) The CDC13-STN1-TEN1 complex stimulates Pol alpha activity by promoting RNA priming and primase-to-polymerase switch. *Nat. Commun.*, **5**, 5762.
12. Schimmel,J., Munoz-Subirana,N., Kool,H., van Schendel,R. and Tijsterman,M. (2021) Small tandem DNA duplications result from CST-guided Pol alpha-primase action at DNA break termini. *Nat. Commun.*, **12**, 4843.
13. Lyu,X., Sang,P.B. and Chai,W. (2021) CST in maintaining genome stability: beyond telomeres. *DNA Repair (Amst.)*, **102**, 103104.
14. Lyu,X., Lei,K.H., Biak Sang,P., Shiva,O., Chastain,M., Chi,P. and Chai,W. (2021) Human CST complex protects stalled replication forks by directly blocking MRE11 degradation of nascent-strand DNA. *EMBO J.*, **40**, e103654.
15. Mirman,Z., Lottersberger,F., Takai,H., Kibe,T., Gong,Y., Takai,K., Bianchi,A., Zimmermann,M., Durocher,D. and de Lange,T. (2018) 53BP1-RIF1-shieldin counteracts DSB resection through CST- and Polalpha-dependent fill-in. *Nature*, **560**, 112–116.
16. Bhattacharjee,A., Wang,Y., Diao,J. and Price,C.M. (2017) Dynamic DNA binding, junction recognition and G4 melting activity underlie the telomeric and genome-wide roles of human CST. *Nucleic Acids Res.*, **45**, 12311–12324.
17. Schuck,P.L., Ball,L.E. and Stewart,J.A. (2021) The DNA-binding protein CST associates with the cohesin complex and promotes chromosome cohesion. *J. Biol. Chem.*, **297**, 101026.
18. Chastain,M., Zhou,Q., Shiva,O., Fadri-Moskwik,M., Whitmore,L., Jia,P., Dai,X., Huang,C., Ye,P. and Chai,W. (2016) Human CST facilitates genome-wide RAD51 recruitment to GC-Rich repetitive sequences in response to replication stress. *Cell Rep.*, **16**, 1300–1314.
19. Wang,F., Stewart,J.A., Kasbek,C., Zhao,Y., Wright,W.E. and Price,C.M. (2012) Human CST has independent functions during telomere duplex replication and C-strand fill-in. *Cell Rep.*, **2**, 1096–1103.
20. Bryan,C., Rice,C., Harkisheimer,M., Schultz,D.C. and Skordalakes,E. (2013) Structure of the human telomeric Stn1-Ten1 capping complex. *PLoS One*, **8**, e66756.
21. Lim,C.J., Barbour,A.T., Zaug,A.J., Goodrich,K.J., McKay,A.E., Wuttke,D.S. and Cech,T.R. (2020) The structure of human CST reveals a decameric assembly bound to telomeric DNA. *Science*, **368**, 1081–1085.
22. Yu,E.Y., Sun,J., Lei,M. and Lue,N.F. (2012) Analyses of Candida Cdc13 orthologues revealed a novel OB fold dimer arrangement, dimerization-assisted DNA binding, and substantial structural differences between Cdc13 and RPA70. *Mol. Cell. Biol.*, **32**, 186–198.
23. Mason,M., Wanat,J.J., Harper,S., Schultz,D.C., Speicher,D.W., Johnson,F.B. and Skordalakes,E. (2013) Cdc13 OB2 dimerization required for productive Stn1 binding and efficient telomere maintenance. *Structure*, **21**, 109–120.
24. Mitchell,M.T., Smith,J.S., Mason,M., Harper,S., Speicher,D.W., Johnson,F.B. and Skordalakes,E. (2010) Cdc13 N-terminal dimerization, DNA binding, and telomere length regulation. *Mol. Cell. Biol.*, **30**, 5325–5334.
25. Wu,Z.J., Liu,J.C., Man,X., Gu,X., Li,T.Y., Cai,C., He,M.H., Shao,Y., Lu,N., Xue,X. *et al.* (2020) Cdc13 is predominant over Stn1 and Ten1 in preventing chromosome end fusions. *Elife*, **9**, e53144.
26. Li,S., Makovets,S., Matsuguchi,T., Blethrow,J.D., Shokat,K.M. and Blackburn,E.H. (2009) Cdk1-dependent phosphorylation of Cdc13 coordinates telomere elongation during cell-cycle progression. *Cell*, **136**, 50–61.
27. Taggart,A.K., Teng,S.C. and Zakian,V.A. (2002) Est1p as a cell cycle-regulated activator of telomere-bound telomerase. *Science*, **297**, 1023–1026.
28. He,Q., Lin,X., Chavez,B.L., Agrawal,S., Lusk,B.L. and Lim,C.J. (2022) Structures of the human CST-Polalpha-primase complex bound to telomere templates. *Nature*, **608**, 826–832.
29. Cai,S.W., Zinder,J.C., Svetlov,V., Bush,M.W., Nudler,E., Walz,T. and de Lange,T. (2022) Cryo-EM structure of the human CST-Polα/primase complex in a recruitment state. *Nat. Struct. Mol. Biol.*, **29**, 813–819.
30. Lin,Y.Y., Li,M.H., Chang,Y.C., Fu,P.Y., Ohniwa,R.L., Li,H.W. and Lin,J.J. (2021) Dynamic DNA shortening by telomere-Binding protein Cdc13. *J. Am. Chem. Soc.*, **143**, 5815–5825.
31. Lewis,K.A., Pfaff,D.A., Earley,J.N., Altschuler,S.E. and Wuttke,D.S. (2014) The tenacious recognition of yeast telomere sequence by Cdc13 is fully exerted by a single OB-fold domain. *Nucleic. Acids. Res.*, **42**, 475–484.
32. Ge,Y., Wu,Z., Chen,H., Zhong,Q., Shi,S., Li,G., Wu,J. and Lei,M. (2020) Structural insights into telomere protection and homeostasis regulation by yeast CST complex. *Nat. Struct. Mol. Biol.*, **27**, 752–762.
33. Lue,N.F., Zhou,R., Chico,L., Mao,N., Steinberg-Neifach,O. and Ha,T. (2013) The telomere capping complex CST has an unusual stoichiometry, makes multipartite interaction with G-Tails, and unfolds higher-order G-tail structures. *PLos Genet.*, **9**, e1003145.
34. Qian,W., Wang,J., Jin,N.-N., Fu,X.-H., Lin,Y.-C., Lin,J.-J. and Zhou,J.-Q. (2009) Ten1p promotes the telomeric DNA-binding activity of Cdc13p: implication for its function in telomere length regulation. *Cell Res.*, **19**, 849–863.
35. García-Nafría,J., Watson,J.F. and Greger,I.H. (2016) IVA cloning: a single-tube universal cloning system exploiting bacterial in vivo assembly. *Sci. Rep.*, **6**, 27459.
36. Studier,F.W. (2005) Protein production by auto-induction in high density shaking cultures. *Protein Expr Purif*, **41**, 207–234.
37. Schuck,P. (2000) Size-Distribution analysis of macromolecules by sedimentation velocity ultracentrifugation and lamm equation modeling. *Biophys. J.*, **78**, 1606–1619.
38. Laue,T.M., Shah,B.D., Ridgeway,T.M. and Pelletier,S.L. (1992) Computer-aided interpretation of sedimentation data for proteins. In: Harding,S.E., Rowe,A.J. and Horton,J.C. (eds). *Analytical Ultracentrifugation in Biochemistry and Polymer Science*. Royal Society of Chemistry, Cambridge, pp. 90–125.
39. Van Der Heijden,T., Seidel,R., Modesti,M., Kanaar,R., Wyman,C. and Dekker,C. (2007) Real-time assembly and disassembly of human RAD51 filaments on individual DNA molecules. *Nucleic Acids Res.*, **35**, 5646–5657.
40. Fili,N., Mashanov,G.I., Toseland,C.P., Batters,C., Wallace,M.I., Yeeles,J.T.P., Dillingham,M.S., Webb,M.R. and Molloy,J.E. (2010) Visualizing helicases unwinding DNA at the single molecule level. *Nucleic Acids Res.*, **38**, 4448–4457.
41. Pastrana,C.L., Carrasco,C., Akhtar,P., Leuba,S.H., Khan,S.A. and Moreno-Herrero,F. (2016) Force and twist dependence of RepC nicking activity on torsionally-constrained DNA molecules. *Nucleic Acids Res.*, **44**, 8885–8896.
42. Kemmerich,F.E., Kasaciunaite,K. and Seidel,R. (2016) Modular magnetic tweezers for single-molecule characterizations of helicases. *Methods*, **108**, 4–13.
43. Carrasco,C., Gilhooly,N.S., Dillingham,M.S. and Moreno-Herrero,F. (2013) On the mechanism of recombination hotspot scanning during

double-stranded DNA break resection. *Proc. Natl. Acad. Sci. U.S.A.*, **110**, E2562–E2571.
44. Strick,T.R., Allemand,J.F., Bensimon,D. and Croquette,V. (1998) Behavior of supercoiled DNA. *Biophys. J.*, **74**, 2016–2028.
45. Zordan,R.E., Ren,Y., Pan,S.J., Rotondo,G., De Las Peñas,A., Iluore,J. and Cormack,B.P. (2013) Expression plasmids for use in Candida glabrata. *G3 (Bethesda)*, **3**, 1675–1686.
46. Kachouri-Lafond,R., Dujon,B., Gilson,E., Westhof,E., Fairhead,C. and Teixeira,M.T. (2009) Large telomerase RNA, telomere length heterogeneity and escape from senescence in Candida glabrata. *FEBS Lett.*, **583**, 3605–3610.
47. Zahid,S., Aloe,S., Sutherland,J.H., Holloman,W.K. and Lue,N.F. (2022) Ustilago maydis telomere protein Pot1 harbors an extra N-terminal OB fold and regulates homology-directed DNA repair factors in a dichotomous and context-dependent manner. *PLoS Genet.*, **18**, e1010182.
48. Mirdita,M., Schutze,K., Moriwaki,Y., Heo,L., Ovchinnikov,S. and Steinegger,M. (2022) ColabFold: making protein folding accessible to all. *Nat. Methods*, **19**, 679–682.
49. Evans,R., O'Neill,M., Pritzel,A., Antropova,N., Senior,A., Green,T., Žídek,A., Bates,R., Blackwell,S., Yim,J. *et al.* (2022) Protein complex prediction with AlphaFold-Multimer. bioRxiv doi: https://doi.org/10.1101/2021.10.04.463034, 10 March 2022, preprint: not peer reviewed.
50. Jumper,J., Evans,R., Pritzel,A., Green,T., Figurnov,M., Ronneberger,O., Tunyasuvunakool,K., Bates,R., Žídek,A., Potapenko,A. *et al.* (2021) Highly accurate protein structure prediction with AlphaFold. *Nature*, **596**, 583–589.
51. Goddard,T.D., Huang,C.C., Meng,E.C., Pettersen,E.F., Couch,G.S., Morris,J.H. and Ferrin,T.E. (2018) UCSF ChimeraX: meeting modern challenges in visualization and analysis. *Protein Sci.*, **27**, 14–25.
52. Sievers,F., Wilm,A., Dineen,D., Gibson,T.J., Karplus,K., Li,W., Lopez,R., McWilliam,H., Remmert,M., Söding,J. *et al.* (2011) Fast, scalable generation of high-quality protein multiple sequence alignments using Clustal Omega. *Mol. Syst. Biol.*, **7**, 539.
53. Altschul,S.F., Gish,W., Miller,W., Myers,E.W. and Lipman,D.J. (1990) Basic local alignment search tool. *J. Mol. Biol.*, **215**, 403–410.
54. Robert,X. and Gouet,P. (2014) Deciphering key features in protein structures with the new endscript server. *Nucleic. Acids. Res.*, **42**, W320–W324.
55. Hang,L.E., Liu,X., Cheung,I., Yang,Y. and Zhao,X. (2011) SUMOylation regulates telomere length homeostasis by targeting Cdc13. *Nat. Struct. Mol. Biol.*, **18**, 920–926.
56. Balaguer,F.A., Aicart-Ramos,C., Fisher,G.L., de Bragança,S., Martin-Cuevas,E.M., Pastrana,C.L., Dillingham,M.S. and Moreno-Herrero,F. (2021) CTP promotes efficient ParB-dependent DNA condensation by facilitating one-dimensional diffusion from parS. *Elife* , **10**, e67554.
57. Taylor,J.A., Pastrana,C.L., Butterer,A., Pernstich,C., Gwynn,E.J., Sobott,F., Moreno-Herrero,F. and Dillingham,M.S. (2015) Specific and non-specific interactions of ParB with DNA: implications for chromosome segregation. *Nucleic. Acids. Res.*, **43**, 719–731.
58. Hormeno,S., Wilkinson,O.J., Aicart-Ramos,C., Kuppa,S., Antony,E., Dillingham,M.S. and Moreno-Herrero,F. (2022) Human HELB is a processive motor protein that catalyzes RPA clearance from single-stranded DNA. *Proc. Natl. Acad. Sci. U.S.A.*, **119**, e2112376119.
59. Mitton-Fry,R.M., Anderson,E.M., Hughes,T.R., Lundblad,V. and Wuttke,D.S. (2002) Conserved structure for single-stranded telomeric DNA recognition. *Science*, **296**, 145–147.
60. Mitton-Fry,R.M., Anderson,E.M., Theobald,D.L., Glustrom,L.W. and Wuttke,D.S. (2004) Structural basis for telomeric single-stranded DNA recognition by yeast Cdc13. *J. Mol. Biol.*, **338**, 241–255.
61. Wellinger,R.J. and Zakian,V.A. (2012) Everything you ever wanted to know about saccharomyces cerevisiae telomeres: beginning to end. *Genetics*, **191**, 1073–1105.
62. Wellinger,R.J. (2009) The CST complex and Telomere maintenance: the exception becomes the rule. *Mol. Cell*, **36**, 168–169.
63. Mersaoui,S.Y., Bonnell,E. and Wellinger,R.J. (2018) Nuclear import of Cdc13 limits chromosomal capping. *Nucleic Acids Res.*, **46**, 2975–2989.
64. Culotti,J. and Hartwell,L.H. (1971) Genetic control of the cell division cycle in yeast: 3. Seven genes controlling nuclear division. *Exp. Cell. Res.*, **67**, 389–401.
65. Yates,L.A., Aramayo,R.J., Pokhrel,N., Caldwell,C.C., Kaplan,J.A., Perera,R.L., Spies,M., Antony,E. and Zhang,X. (2018) A structural and dynamic model for the assembly of Replication Protein A on single-stranded DNA. *Nat. Commun.*, **9**, 5447.
66. Mersaoui,S.Y. and Wellinger,R.J. (2019) Fine tuning the level of the Cdc13 telomere-capping protein for maximal chromosome stability performance. *Curr. Genet.*, **65**, 109–118.
67. Larrivée,M., LeBel,C. and Wellinger,R.J. (2004) The generation of proper constitutive G-tails on yeast telomeres is dependent on the MRX complex. *Genes Dev.*, **18**, 1391–1396.
68. Osterhage,J.L., Talley,J.M. and Friedman,K.L. (2006) Proteasome-dependent degradation of Est1p regulates the cell cycle–restricted assembly of telomerase in *Saccharomyces cerevisiae*. *Nat. Struct. Mol. Biol.*, **13**, 720–728.
69. Dionne,I. and Wellinger,R.J. (1996) Cell cycle-regulated generation of single-stranded G-rich DNA in the absence of telomerase. *Proc. Natl. Acad. Sci. U.S.A.*, **93**, 13902–13907.